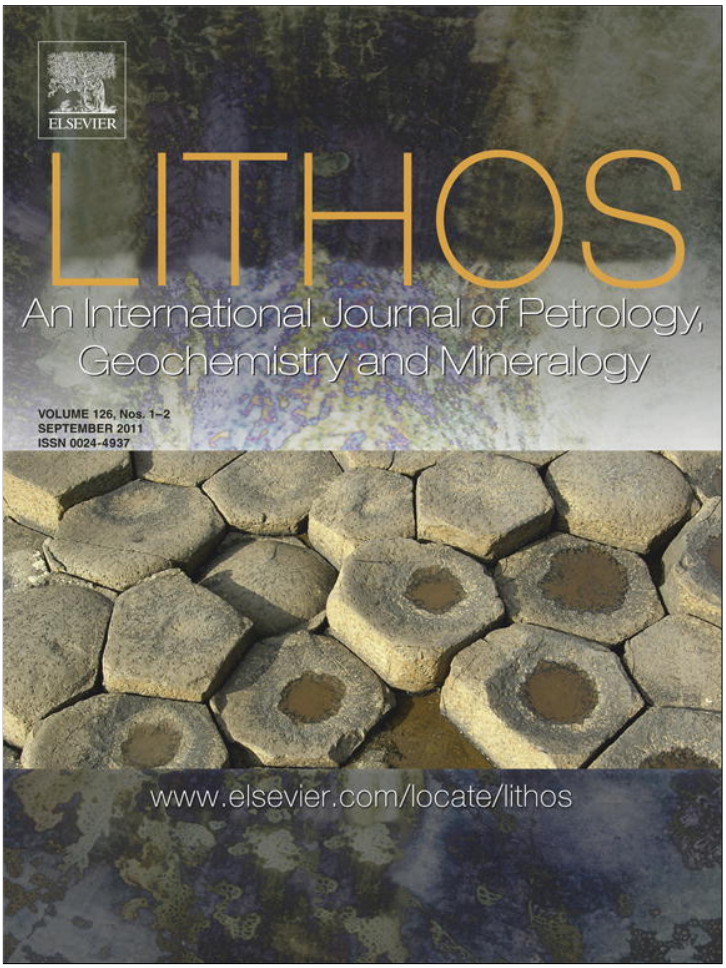

Lithos 126 (2011) 22–41

Contents lists available at ScienceDirect

Lithos

journal homepage: www.elsevier.com/locate/lithos

The generation of high Sr/Y plutons following Late Jurassic arc–arc collision, Blue Mountains province, NE Oregon

Joshua J. Schwartz [a,*], Kenneth Johnson [b], Elena A. Miranda [c], Joseph L. Wooden [d]

[a] Department of Geological Sciences, California State University Northridge, Northridge, CA, 91330, USA
[b] Department of Natural Sciences, University of Houston- Downtown, Houston, TX 77002, USA
[c] Department of Geological Sciences, California State University Northridge, Northridge, CA, 91330, USA
[d] Stanford University, Stanford, CA, 94305, USA

ARTICLE INFO

Article history:
Received 4 December 2010
Accepted 12 May 2011
Available online 23 May 2011

Keywords:
High Sr/Y plutons
Arc–arc collision
Late Jurassic orogeny
U–Pb zircon geochronology
Zircon Hf isotope geochemistry
Blue Mountains province

ABSTRACT

High Sr/Y plutons (Sr/Y>40) occupy large areas in ancient and modern orogenic belts, yet considerable controversy exists regarding mechanisms of their generation, the tectonic settings in which they form, and their relationship to contractional deformation through time. In the Blue Mountains province (NE Oregon), a suite of Late Jurassic (148–145 Ma), high Sr/Y plutons intrude Middle Jurassic (162–157 Ma), low Sr/Y (<40) arc-related lavas and plutons in the Dixie Butte area immediately after widespread Late Jurassic arc–arc collision (159–154 Ma). Early, pre- to syn-kinematic low Sr/Y lavas and plutons (162–157 Ma) have flat to slightly enriched light rare earth element (REE) abundances, low Sr (<400 ppm) and Sr/Y values (<40), and strongly positive initial epsilon Hf values (+10.1 to +12.3: 2σ weighted average). Ce/Y values from basalts and gabbros yield a maximum crustal thickness of ~23 km. These geochemical and isotopic features suggest derivation from a depleted-mantle source and/or shallow-level (≪40 km) melting of pre-existing island arc crust with little to no evolved crustal input. In contrast, post-kinematic high Sr/Y plutons (148–145 Ma) are more compositionally restricted (tonalite–trondhjemite–granodiorite) and display depleted heavy REE abundances, an absence of Eu anomalies, elevated Sr (>600 ppm) and Sr/Y values (>40), and positive initial epsilon Hf values (+10.5 to +7.8: 2σ weighted average). These geochemical and isotopic results are consistent with geochemical models suggesting derivation from partial melting of island arc crust in the presence of a plagioclase-poor to absent, clinopyroxene + hornblende + garnet-bearing source (depths >35–40 km).

We propose that the transition from low Sr/Y to high Sr/Y magmatism resulted from orogenic thickening of island arc crust in the Dixie Butte area during Late Jurassic arc–arc collision between the Olds Ferry and Wallowa island arcs at 159–154 Ma. This fundamental change in crustal structure influenced post-orogenic magmatism and resulted in a relatively brief (~3 myr: 148–145 Ma) episode of high Sr/Y magmatism. Other high Sr/Y plutons occur throughout the US sector of the western North American Cordillera (e.g., Salmon River suture zone, Klamath Mountains, Peninsular Ranges) and closely follow major contractional events involving arc–arc and arc–continent collisions.

1. Introduction

Magmas with high Na, Al, Sr, Sr/Y and low Y geochemical characteristics (high Sr/Y plutons: Tulloch and Kimbrough, 2003) are common features in modern and ancient convergent margin settings, and play an integral role in the construction and differentiation of continental crust (e.g., Drummond and Defant, 1990; Gromet and Silver, 1987; Silver and Chappell, 1988; Smithies, 2000). In Phanerozoic convergent margin settings, high Sr/Y magmas (Sr/Y>40) principally occur in two distinct magmatic associations: (1) as mafic–intermediate volcanic rocks commonly associated with subduction zone settings (often termed 'adakites'); and (2) as diorite–tonalite–granodiorite plutons and batholiths frequently spatially and temporally associated with coeval belts of low Na, Al and Sr, and high Y (low Sr/Y) rocks [see Moyen (2009) for a detailed discussion of high Sr/Y rocks]. In the latter case, high Sr/Y batholiths and plutons occupy large areas (up to 15,000 km^2) in convergent margin orogenic belts (e.g., Peninsular Ranges batholith, Separation Point suite, Cordillera Blanca batholith: Ague and Brimhall, 1988; Gastil, 1975; Gromet and Silver, 1987; Muir et al., 1997, 1998; Petford and Atherton, 1996; Silver et al., 1979; Taylor and Silver, 1978; Tulloch, 1983, 1988; Tulloch and Rabone, 1993), and signify major fluxes (up to 75–100 km^3/km/myr: Tulloch and Kimbrough, 2003) of unusually high Sr/Y magmas whereby plagioclase is minor to absent and garnet is a

* Corresponding author.
E-mail address: joshua.j.schwartz@gmail.com (J.J. Schwartz).

0024-4937/$ – see front matter © 2011 Elsevier B.V. All rights reserved.
doi:10.1016/j.lithos.2011.05.005

residual phase. Such high Sr/Y magmas are also intimately associated with ore mineralization in convergent margin settings worldwide (Chiaradia et al., 2004; Kay and Mpodozis, 2001; Tulloch and Rabone, 1993).

The widespread occurrence of high Sr/Y magmas raises a number of questions regarding their origin (e.g., partial melting of subducted slab or lower arc crust) and the tectonic setting in which they occur. Although numerous studies have investigated the geochemical characteristics of high Sr/Y magmas in Phanerozoic through Archean settings (e.g., Drummond and Defant, 1990; Gromet and Silver, 1987; Martin, 1999; Smithies, 2000; Tulloch and Kimbrough, 2003; Wang et al., 2005, 2007, 2008; Xu et al., 2009), few studies have focused on the role of deformation and crustal thickening by collision (e.g., arc–arc and/or arc–continent collision involving tectonically buoyant rocks: Cloos, 1993) in their genesis (c.f., Chung et al., 2003, 2005, 2009; Guo et al., 2007a, 2007b). For example, what role does episodic collision and associated crustal thickening play in the distribution and triggering of high Sr/Y magmatism in convergent margin settings? Are some high Sr/Y magmas generated through collision and partial melting of orogenically thickened crust in the garnet–amphibole stability field? And do high Sr/Y magmas represent new additions to evolving continental crust, or do they represent recycling of pre-existing continental lithosphere? The generation of these magmas has important implications for the evolution of continental lithosphere from the Archean to the Phanerozoic (c.f., Rudnick, 1995).

In this manuscript, we investigate the magmatic development of Late Jurassic high Sr/Y plutons in the Dixie Butte area of the Blue Mountains province (BMP) in northeastern Oregon (Figs. 1 and 2). In this region of the western North American Cordillera, high Sr/Y plutonism closely follows a widespread regional contractional event interpreted to signify the terminal collision of the Olds Ferry and Wallowa island arcs (Avé Lallemant, 1995; Schwartz et al., 2010, 2011). The close spatial and temporal relationships between the generation of high Sr/Y plutons and arc–arc collision allow us to investigate the mechanisms of high Sr/Y magma generation in a collisional orogenic belt and the role of high Sr/Y plutons in the creation of juvenile crust. Our combined structural, geochemical and geochronological study documents that Middle to early Late Jurassic, low Sr/Y plutons and lavas (162–157 Ma) were emplaced into relatively thin arc crust (~23 km) and formed by partial melting of shallow mafic arc crust and/or depleted mantle. Following arc–arc collision at 159–154 Ma, partial melting of orogenically thickened (>35 km) mafic arc crust resulted in a second phase of short-lived, high Sr/Y magmatism from 148 to 145 Ma. Similar high Sr/Y plutons also occur in the Klamath Mountains, Peninsular Ranges and Salmon River suture zone, recording episodic, orogen-wide generation of high Sr/Y melts following widespread Late Jurassic to Early Cretaceous collisional events along the western North American margin.

2. Geologic framework of the Blue Mountains province

The Blue Mountains province of northeastern Oregon and western Idaho (Fig. 1) consists of three distinct terranes (Fig. 1) (Brooks and Vallier, 1978; Dickinson and Thayer, 1978; Dickinson et al., 1979; LaMaskin et al., 2009a; Schwartz et al., 2011; Silberling et al., 1987; Walker, 1986). These terranes include the Wallowa and Olds Ferry island arc-related terranes, Baker oceanic mélange terrane, and Izee fore-arc or collisional basin (Dickinson, 1979; Dickinson and Thayer, 1978; Dorsey and LaMaskin, 2007; LaMaskin et al., 2008, 2011). The Wallowa terrane is a composite island–arc system consisting of a Permian island–arc complex overlain and/or intruded by Upper Triassic to Lower Jurassic sedimentary, volcanic, volcaniclastic, and plutonic rocks (Kays et al., 2006; Vallier, 1977, 1995; Vallier and Batiza, 1978; Vallier et al., 1977). Plutonic rocks range in age from ~264–215 Ma (Kurz et al., 2009; Schwartz et al., 2010; Walker, 1986, 1995). The Olds Ferry island–arc terrane is partially coeval with the Wallowa terrane and consists chiefly of Middle Triassic to Lower Jurassic weakly metamorphosed, volcanic, volcaniclastic and sedimentary rocks of the Huntington Formation (Brooks and Vallier, 1978; Tumpane and Schmitz, 2009). These volcanogenic rocks are dominantly andesitic, but range from basalt to rhyolite. Arc-related plutonism and volcanic activity range from Middle Triassic to Early Jurassic (Tumpane and Schmitz, 2009; Walker, 1995).

The Baker terrane lies between the Wallowa and Olds Ferry island–arc terranes (Fig. 1). It is the oldest and most structurally complex terrane in the BMP (Blome and Nestell, 1991; Carpenter and Walker, 1992; Ferns and Brooks, 1995; Nestell, 1983; Nestell and Nestell, 1998; Nestell and Orchard, 2000; Nestell et al., 1995; Schwartz et al., 2010, 2011; Walker, 1986, 1995). Previous workers have recognized three subterranes (Bourne and Greenhorn subterranes and Burnt River Schist; Fig. 1) (Ferns and Brooks, 1995; Schwartz et al., 2010, 2011). The dominant lithologic unit of the Bourne subterrane is the Elkhorn Ridge Argillite (Coward, 1983; Gilluly, 1937; Pardee and Hewett, 1914), which contains Permian to Early Jurassic chert and argillite with lesser blocks of coherent, bedded argillite and ribbon chert (Blome et al., 1986; Coward, 1983; Ferns et al., 1987). The Burnt River Schist (Ashley, 1995; Gilluly, 1937) is a heterogeneous suite of rocks chiefly dominated by fine-grained metasedimentary rocks (e.g., slaty argillite and siliceous phyllite) but also includes mappable bodies of greenschist-facies metavolcanic rocks, mafic to felsic metaplutonic rocks (i.e., Blue Spring Gulch pluton), and impure marble. The Greenhorn subterrane hosts the Dixie Butte Meta-andesite complex and is the focus of this study. It consists of serpentinite-matrix mélange including large blocks of arc-related metaplutonic, metavolcanic (locally pillowed) and metavolcaniclastic rocks, brecciated chert-argillite, and amphibolitic rocks. These rocks are overlain by Permian–Triassic conglomerate, sandstone, argillite, and limestone of the Badger Creek metasedimentary unit (Ferns and Brooks, 1995; Mullen, 1978; Wheeler, 1976).

All three terranes in the BMP (including Izee basin) were folded and faulted by Late Jurassic contractional deformation, which involved the development of widespread, penetrative ~east–west-oriented slaty to spaced cleavage, ~north–south-directed folding, and northward- and southward-dipping reverse and thrust faulting. Age constraints from detrital zircon populations in deformed sedimentary rocks and $^{206}Pb/^{238}U$ zircon ages of post-kinematic fault-stitching plutons bracket contractional deformation between ~159 and 154 Ma (Schwartz et al., 2011). The widespread ~N–S-directed contractional features in the BMP have been interpreted to record a short-lived episode of deformation related to the early Late Jurassic, terminal collision of the distal, Wallowa island arc with the fringing, continental-margin Olds Ferry island arc (Avé Lallemant, 1995; Schwartz et al., 2010, 2011). Magmatism in the BMP spanned Late Jurassic contraction, occurring syn-kinematically between 162 and 154 Ma, and post kinematically between 148 and 141 Ma (Fig. 3 and Table 1) (Johnson and Barnes, 2002; Johnson and Schwartz, 2009; Johnson et al., 2007; Schwartz and Johnson, 2009; Unruh et al., 2008; Walker, 1986, 1989, 1995).

2.1. Geology of the Dixie Butte Meta-andesite complex

The Dixie Butte Meta-andesite complex, located in the Greenhorn subterrane of the Baker terrane, is exposed over >80 km^2, making it one of the largest continuous volcanogenic complexes in the BMP (Brooks et al., 1984; Ferns and Brooks, 1995). Pre-Tertiary rocks consist of serpentinite-matrix mélange (including knockers of chert argillite), the Permian–Triassic Badger Creek metasedimentary unit, Dixie Butte Meta-andesite, and two suites of Middle and Late Jurassic plutons (Fig. 2). The Dixie Butte Meta-andesite consists of a lower sequence of tuffaceous sedimentary rocks and volcaniclastic breccias, and an upper sequence of flow rocks and subordinate

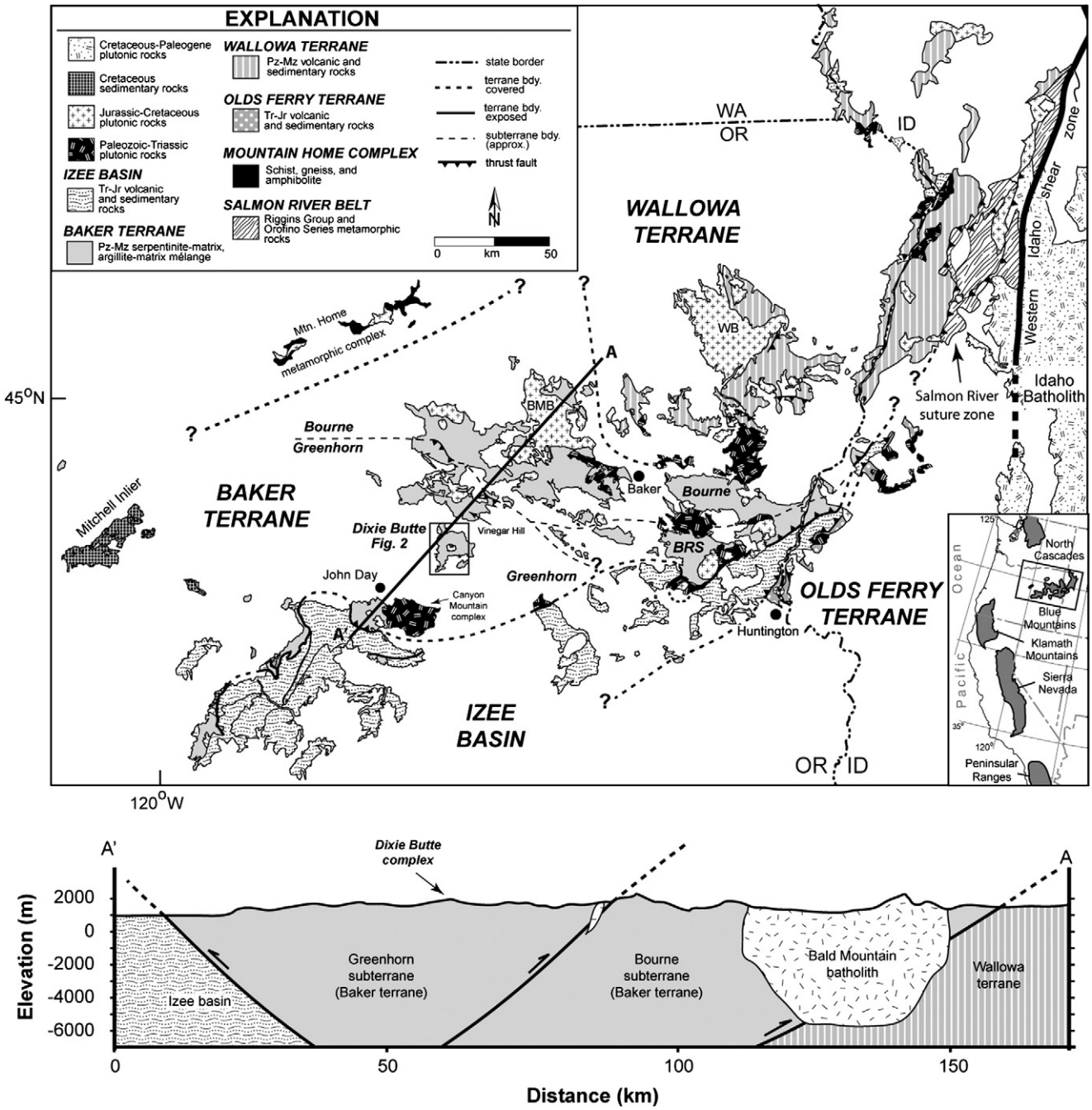

Fig. 1. Regional map of the Blue Mountains province, northeastern Oregon and western Idaho, showing the locations of the various terranes and subterranes (modified from LaMaskin et al., 2009b). Location of Fig. 2 is shown for reference. Inset map shows location of the Blue Mountains province with respect to other Paleozoic–Mesozoic accreted terranes of the North American Cordillera. BMB = Bald Mountain batholith; WB = Wallowa batholith.

volcaniclastic breccias and sills. Pre- to syn-kinematic, gabbro–diorite–trondhjemite plutons intrude the Dixie Butte Meta-andesite and are typically altered at greenschist-facies conditions. A second, distinct suite of post-kinematic and unaltered tonalites, trondhjemites and dacites occurs in the western portion of the Dixie Butte area. These plutons and the Dixie Butte Meta-andesite are the focus of this study.

3. Methods

Samples for major- and trace-element geochemistry were selected to represent the major plutonic rocks of the Dixie Butte area and were collected from the least altered and least deformed rocks to minimize effects of greenschist-facies alteration (DR Table 1). Rock chips were handpicked at the University of Alabama, and weathered surfaces and veins were discarded. Major and trace elements were analyzed by XRF and ICPMS at the University of Alabama, and by ICP-OES at the University of Houston-Downtown (Table 2; DR Table 2; DR Figs. 1–4). U–Pb zircon geochronology was conducted at the Stanford-USGS SHRIMP-RG facility and at the Arizona LaserChron Center (DR Tables 3 and 4). Zircon Hf isotope analyses were conducted at the University of Arizona on a subset of the U–Pb zircon samples (DR Table 5). Analytical details are given in Appendix A.

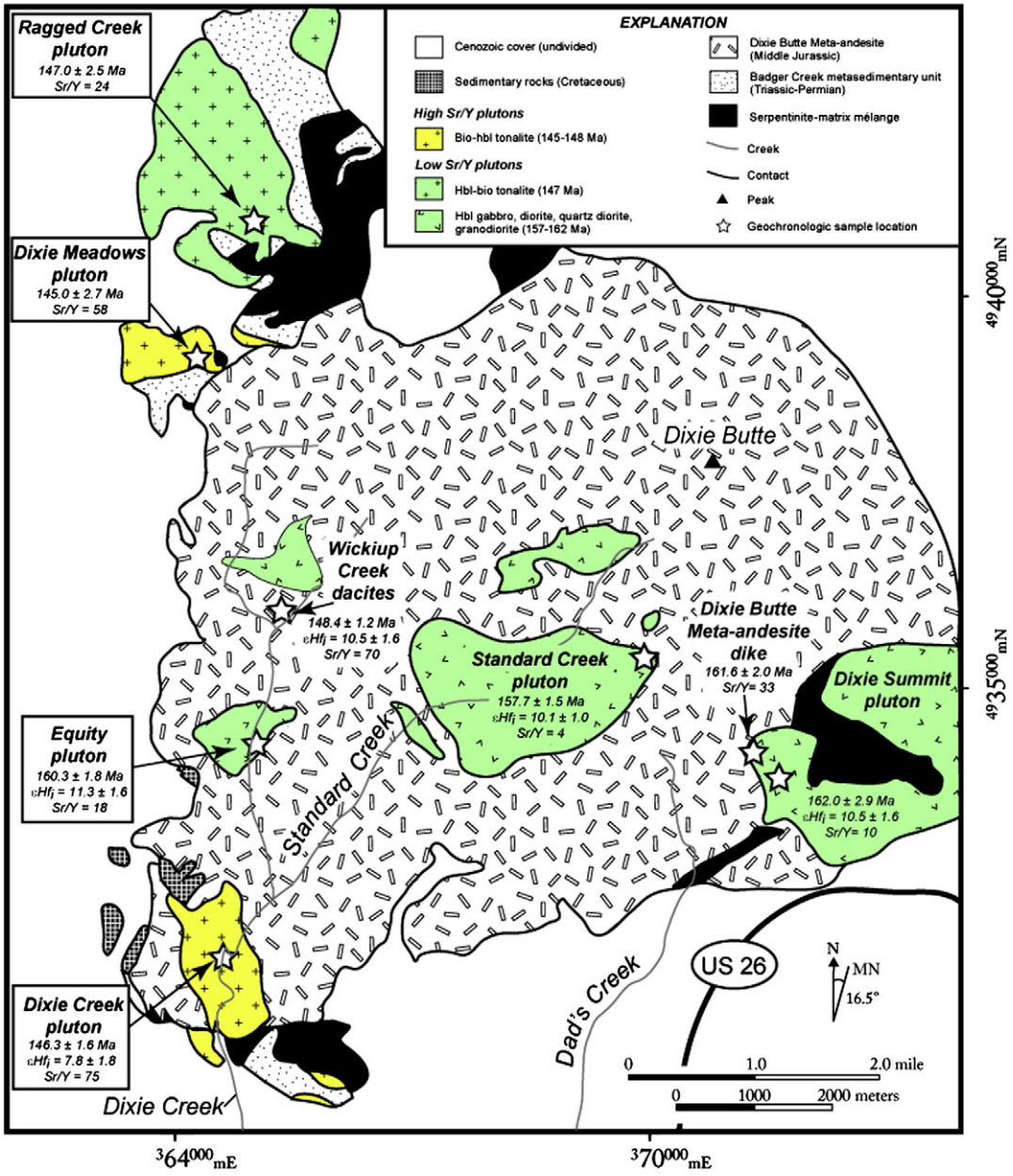

Fig. 2. Simplified geologic map of the Dixie Butte area [Greenhorn subterrane of the Baker terrane (after Brooks et al., 1984)]. Locations of samples discussed in text are show by stars.

4. Results

4.1. Field and petrographic observations

4.1.1. Dixie Butte Meta-andesite (Middle Jurassic)

The basal portion of the Dixie Butte Meta-andesite is best exposed on Dad's Creek (Fig. 2) and consists of ~2000–2200 feet of thick-bedded andesitic lithic tuff, lithic–clast volcaniclastic breccia, pepperite, tuffaceous sandstone, graphitic argillite, and pebble conglomerate. Basal sedimentary rocks appear to be unconformably deposited over older brecciated chert argillites which contain Wolfcampian (i.e., Late Permian) radiolarians (Schwartz et al., 2011). Dominant lithic clasts in the pebble conglomerates are trachytic basaltic andesite with subordinate diorite, microdiorite, reworked lithic tuff, and fine-grained chert and argillite (Fig. 4A). Lithic clasts are subrounded to angular in shape. Volcanogenic sandstones locally display normally graded bedding (see 'Structural features' below). Argillites and fine- to medium-grained sandstones grade up-section into coarser, lithic–clast volcaniclastic breccias. These rocks are in turn overlain by volcanic flows and tuffs in the upper portion of the Dixie Butte (Fig. 4B).

The upper section of the Dixie Butte Meta-andesite complex consists of green to gray, trachytic plagioclase- and augite-phyric basaltic andesite and andesite flows, subordinate volcaniclastic breccias, keratophyre, dark-gray basalt, and pale-green silicic flows and tuffs (Brooks et al., 1984; Ferns and Brooks, 1995). The primary igneous mineral phases of the volcanic rocks are plagioclase and augite ± apatite ± orthopyroxene ± quartz. Vesicles are common in some rocks and are typically filled with calcite, quartz, and/or chlorite. No pillow structures have been observed. Lavas and volcaniclastic breccias in the upper section are intruded by fine-grained microgabbro and microdiorite sills and dikes with chilled margins. Microgabbro and diorite sills consist of plagioclase + clinopyroxene + hornblende + apatite ± zircon. Basaltic and andesitic dikes are locally observed in the basal section at Dad's Creek and cross-cut mafic plutonic rocks of the Dixie Summit and Equity plutons (see description below). No dikes are observed intruding the tonalite–trondhjemite–granodiorite suite.

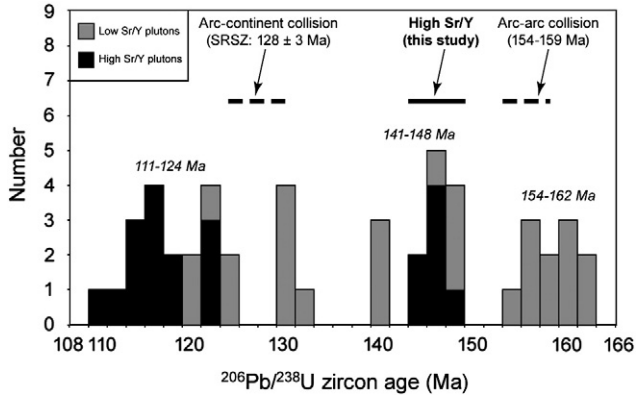

Fig. 3. Histogram of $^{206}Pb/^{238}U$ zircon ages showing three pulses of Middle Jurassic to Early Cretaceous magmatism in the Blue Mountains province (data sources: Johnson and Schwartz, 2009; LaMaskin et al., 2009a, 2009b; Lee, 2004; Manduca et al., 1993; McLelland and Oldow, 2007; Schwartz and Johnson, 2009; Schwartz and Johnson, unpublished data; Snee et al., 2007; Unruh et al., 2008; Walker, 1986). SRSZ: Salmon River suture zone (Getty et al., 1993). Timing of inferred arc–arc collision from Schwartz et al. (in press).

Lavas and dikes typically display low-temperature propylitic alteration with replacement of primary minerals by chlorite, epidote, sphene and carbonate. Pyritic alteration is also common near intrusive contacts with tonalite plutons and subvolcanic porphyries (e.g., Dixie Creek pluton and Wickiup Creek dacite porphyries: Fig. 2). Alteration is typically less intense than other areas of the Greenhorn subterrane (e.g., Ferns and Brooks, 1995) and is highly localized at the meter scale.

4.1.2. Gabbro–diorite–granodiorite suite (162–157 Ma)

Mafic plutonic rocks occur as small (<3 km^2) sheeted intrusions in the east-central (Dixie Summit pluton) and west-central (e.g., Equity pluton) regions of the Dixie Butte area (Fig. 2). These rocks range from gabbro to quartz diorite, and contain the following primary igneous mineral phases: clinopyroxene + plagioclase feldspar ± orthopyroxene + zircon + apatite. Ophitic textures are common in gabbroic and dioritic samples (e.g., Fig. 4C). Primary igneous minerals are often extensively altered (sometimes at and/or near dike and dikelette contacts) to secondary minerals such as chlorite, calcite, albite or actinolite.

Several field relationships suggest a possible consanguineous relationship between the mafic plutonic rocks (e.g., Dixie Summit and Equity plutons) and the Dixie Butte Meta-andesites. Potential comagmatic relationships include: (1) the intrusion of gabbro–diorite into basaltic andesite, (2) fragments of gabbro, diorite, and microdiorite in lithic–clast volcaniclastic breccias throughout the basal section of the Dixie Butte Meta-andesite, and (3) intrusion of fine-grained plagioclase-phyric meta-andesite dikes and dikelettes into the Dixie Summit and Equity plutons (but not into 146-Ma plutons). Possible consanguineous relationships are also supported by whole rock geochemical similarities (see below and DR Figs. 1–4).

Along Standard Creek, a separate intrusive suite occupies the central portion of the Dixie Butte region. Plutonic rocks in this area consist primarily of biotite–hornblende granodiorite that intrude Dixie Butte Meta-andesite flow rocks. Primary igneous mineral phases include quartz, plagioclase feldspar, minor alkali feldspar, hornblende, biotite, zircon, and apatite. Primary minerals are commonly altered to secondary minerals including chlorite, calcite, albite and actinolite.

4.1.3. Tonalite–trondhjemite–granodiorite suite (148–145 Ma)

A second suite of plutonic rocks and subvolcanic porphyries intrude metavolcanic and metasedimentary rocks in the western portion of the Dixie Butte area (see 148–145-Ma rocks in Fig. 2). Plutonic rocks consist of biotite–hornblende tonalite with minor K-feldspar and accessory zircon, sphene, and apatite (e.g., Fig. 4D). Graphic intergrowth of quartz and plagioclase is common. Fine-grained hornblende + plagioclase enclaves are present, though rare in the Dixie Creek pluton and appear to be magmatic in origin. Secondary (deuteric?) alteration of biotite to chlorite is minor, and in general propylitic alteration characteristic of the older 162–517 Ma suite is absent in these rocks.

Strongly porphyritic biotite–hornblende dacites occur in the Wickiup Creek area and form concordant subvolcanic sheets that intrude basalt and basaltic andesite flow rocks of the Dixie Butte Meta-andesite unit. Mineralogically, they are similar to biotite–hornblende tonalites. Although they are interstratified with Dixie Butte Meta-andesites, the Wickiup Creek porphyries are distinguished from the Dixie Butte metavolcanic rocks in that they contain abundant quartz, hornblende and biotite as phenocryst phases.

4.2. Structural features

In the basal portion of Dixie Butte near Dad's Creek, metavolcaniclastic breccias, sandstones, and argillites consistently strike north-northeast and dip moderately to the west-northwest. Normally graded bedding and scour surfaces observed in the metavolcaniclastic breccias indicate an upright orientation. The similar orientation of bedding in the breccias, sandstones, and argillites suggests that the sandstones and argillites are also upright in orientation.

The metasedimentary rocks in the basal portion of Dixie Butte display evidence for tectonic tilting and possibly folding. The consistent orientation of the moderately-dipping beds in the metasedimentary rocks suggests that the entire sequence was rotated or tilted either along faults or by folding. However, folding is suggested by the presence of a penetrative fracture cleavage that is obliquely oriented to bedding. Metavolcaniclastic sandstones and argillites exhibit a penetrative fracture cleavage that strikes south-southeast and dips steeply to the west-southwest, though the cleavage is best developed in the argillite and subdued in the sandstone. The cleavage has a steeper dip than that of the bedding, consistent with the development of axial planar cleavage in the upright limb of a fold. Provided that the fracture cleavage is an axial planar cleavage, this implies that the other fold limb strikes northwest and dips to the northeast, and is located to the northeast of this location. The intersection of the bedding and cleavage defines a

Table 1
Summary of characteristics of Late Jurassic plutonic rocks in the Dixie Butte area, Blue Mountains Province, NE Oregon.

	Rock type	Age (Ma)	Associated volcs?	Associated mafic rocks?	Fe-number	MALI	SiO_2 (range)	Na_2O/K_2O (average)	~Sr (average)	Sr/Y (average)	La/Lu (average)	Epsilon Hf initial (range)
LoSY	Gabbro, hbl ± bio diorite, bio-hbd trondhjemite	162–157	Yes?	Yes	Bimodal: ferroan/ magnesian	Bimodal: alkalic/calcic	68–50	3.4	280	9.1	33	12.3–10.1
HiSY	Bio ± musc. tonalite–granodiorite	148–145	No	Rare	Magnesian	Calcic–calc alkalic	67-64	2.5	765	71	130	10.5–7.8
LoSY	Bio-hbd tonalite	147	No	Rare	Magnesian	Calcic–calc alkalic	61–56	1.8	728	31	76	n.d.

Table 2
Whole rock major and trace element geochemical data.

Laboratory	Dixie Butte Meta-andesites			Dixie Summit pluton		Equity pluton	Standard Creek pluton	Dixie Creek pluton		Ragged Creek pluton		Dixie Meadows pluton
	07DBO1A	07DBO3B	08DBO51	08DBO23	07DBO46	08DBOJ9	07DBO24	07DBO26	08DBO9	08DBOJ13R	09DBO17	08DBOJ12
	UA	UA	UA	UA	UA	UA	UA	UA	UA	UA	UA	UA
SiO_2	55.45	53.54	57.23	51.39	52.81	52.94	66.46	66.08	66.31	60.79	53.50	66.44
TiO_2	1.07	1.23	0.91	1.21	1.01	0.75	0.56	0.45	0.44	0.84	1.02	0.45
Al_2O_3	16.05	18.69	18.25	19.24	19.68	19.00	15.82	16.27	16.14	16.42	18.19	16.31
FeO*	8.08	8.30	7.44	8.62	7.56	6.37	5.95	4.00	3.85	6.41	8.77	3.65
MnO	0.16	0.18	0.14	0.17	0.14	0.11	0.11	0.06	0.06	0.13	0.16	0.06
MgO	8.41	5.20	3.15	4.93	4.82	5.32	0.68	1.67	1.65	2.99	4.34	1.78
CaO	9.26	8.68	7.83	10.05	9.79	10.06	2.18	4.24	4.05	5.37	7.95	4.14
Na_2O	2.39	3.33	3.84	3.99	3.98	3.63	6.00	4.26	4.15	3.43	3.24	4.22
K_2O	0.31	0.76	0.83	0.39	0.63	1.12	2.20	2.37	2.47	2.52	1.68	1.76
P_2O_5	0.20	0.21	0.23	0.15	0.11	0.12	0.20	0.14	0.13	0.22	0.27	0.12
L.O.I.	3.29	2.92	3.66	1.62	2.04	2.45	1.64	1.02	1.25	0.73	0.86	1.21
Total	101.38	100.13	99.86	100.16	100.53	99.42	100.17	99.53	99.25	99.11	99.12	98.92
Fe#	0.49	0.61	0.70	0.64	0.61	0.55	0.90	0.71	0.70	0.68	0.67	0.67
MALI	−6.47	−4.58	−3.16	−5.67	−5.14	−5.34	6.00	2.39	2.60	0.59	−3.02	1.87
V	167.89	204.20	173.20	137.60	134.40	163.40	25.60	72.00	66.20	159.00	274.73	71.00
Cr	440.01	185.20	9.00	45.60	69.40	109.60	b.d.	15.00	9.00	28.00	74.69	22.20
Ni	166.31	75.40	5.60	32.00	27.80	73.20	5.00	9.20	8.40	10.40	45.63	8.80
Cu	149.07	72.40	9.40	12.40	60.60	32.00	12.00	8.60	6.20	12.20	12.35	3.20
Zn	77.49	88.40	73.00	93.20	89.80	43.40	52.60	21.00	21.40	72.60	83.09	28.80
Rb	16.20	18.60	14.20	9.60	13.60	30.20	28.80	66.80	70.80	64.60	38.19	46.60
Sr	221.17	322.20	629.40	340.60	291.80	343.80	155.40	734.20	744.00	567.80	621.84	648.00
Y	24.24	27.80	18.80	25.20	21.40	19.20	57.80	10.20	10.00	23.60	25.89	11.20
Zr	147.35	157.00	122.20	100.60	113.60	118.00	348.00	152.00	153.80	169.00	124.58	151.20
Nb	5.72	6.00	7.20	4.00	3.40	4.60	14.00	10.00	10.40	9.40	7.04	7.40
Ba	193.55	206.80	311.40	116.00	139.60	251.40	581.60	929.80	972.00	879.60	561.66	821.40
Pb	2.24	1.46	3.63	n.d.	1.47	7.43	n.d.	n.d.	3.44	5.88	4.72	3.44
Th	3.60	1.21	1.34	n.d.	0.61	1.39	n.d.	n.d.	4.88	4.69	4.41	3.60
U	0.58	0.32	0.56	n.d.	0.06	0.45	2.00	3.00	2.03	1.72	1.05	1.61
Sc	42.25	29.83	17.26	n.d.	24.46	23.84	n.d.	n.d.	7.40	18.39	30.56	7.14
La	14.27	11.47	11.06	n.d.	6.06	6.29	20.59	19.31	19.50	27.98	18.26	14.49
Ce	30.73	25.31	22.98	n.d.	15.27	13.94	49.02	34.55	33.89	65.60	41.45	27.71
Pr	4.02	3.37	3.08	n.d.	2.17	1.86	6.66	3.73	3.70	7.23	5.41	3.08
Nd	17.47	14.89	12.99	n.d.	10.20	10.30	28.87	13.28	13.31	28.69	23.84	12.15
Sm	4.53	3.80	2.89	n.d.	2.51	2.08	7.48	2.33	2.38	5.33	5.03	2.18
Eu	1.27	1.25	1.07	n.d.	1.09	0.85	1.75	0.70	0.73	1.36	1.35	0.67
Gd	4.96	4.15	2.75	n.d.	3.56	2.36	8.22	1.87	1.94	4.82	5.19	1.80
Tb	0.82	0.69	0.42	n.d.	0.53	0.40	1.38	0.28	0.28	0.81	0.77	0.26
Dy	5.32	4.35	2.54	n.d.	3.42	2.54	9.02	1.62	1.65	4.75	4.60	1.74
Ho	1.10	0.90	0.50	n.d.	0.73	0.66	1.79	0.32	0.31	0.94	0.89	0.40
Er	3.05	2.47	1.42	n.d.	2.11	1.85	5.13	0.89	0.88	2.48	2.50	1.22
Tm	0.42	0.34	0.20	n.d.	0.26	0.27	0.75	0.13	0.13	0.38	0.35	0.17
Yb	2.68	2.15	1.33	n.d.	1.88	1.71	4.98	0.85	0.87	2.25	2.23	1.21
Lu	0.39	0.30	0.20	n.d.	0.24	0.25	0.70	0.12	0.13	0.35	0.33	0.17
Sr/Y	9.12	11.59	33.48	13.52	13.64	17.91	2.69	71.98	74.40	24.06	24.02	57.86
La/Yb	5.32	5.35	8.33	n.d.	3.22	3.69	4.14	22.67	22.46	12.45	8.19	11.96

lineation that is parallel to the fold axis, consistent with a northwest plunge of the suspected fold. Based on the orientation of the axial planar cleavage, the axial plane of the suspected fold strikes south-southeast, consistent with tectonic shortening in a NE–SW direction.

4.3. U–Pb zircon geochronology

4.3.1. Metavolcanic and gabbro–diorite–granodiorite suite (162–157 Ma)

Samples selected for U–Pb zircon dating from the gabbro–diorite–trondhjemite suite include a diorite from the Dixie Summit pluton (07DBO46), a meta-andesite dike that intrudes the Dixie Summit pluton (08DBO51), a strongly altered diorite from the Equity pluton (08DBOJ9/10), and a granodiorite from the Standard Creek pluton (07DBO24). Individual zircon spot analyses in general yield concordant ages with minor inherited components (c.f., Figs. 5 and 6 and DR Tables 3 and 4). Due to varying degrees of greenschist-facies alteration, Pb-loss is apparent in several samples and is particularly obvious in the Dixie Summit and Equity plutons. Weak, diffuse oscillatory zoning in these samples (Fig. 5) may reflect Pb-loss (e.g., Connelly, 2001), or original weak oscillatory textures common in zircon crystallized from mafic rocks (e.g., Baines et al., 2009; Grimes et al., 2007, 2009; McLelland et al., 2004; Tomaschek et al., 2003). Consequently, spot analyses that were likely affected by Pb-loss are excluded in weighted-average age calculations (gray spot analyses in Fig. 6). We interpret the weighted-average $^{206}Pb/^{238}U$ age of the gabbro–diorite–granodiorite suite as follows: the Dixie Summit pluton: 162.0 ± 2.0 Ma (MSWD = 2.9) (Fig. 6A); meta-andesite dike: 161.6 ± 2.0 Ma (MSWD = 2.6) (Fig. 6B); the Equity pluton: 160.3 ± 1.8 Ma (MSWD = 3.6) (Fig. 6C); and the Standard Creek pluton: 157.7 ± 1.5 Ma (MSWD = 1.1) (Fig. 6D).

4.3.2. Tonalite–trondhjemite–granodiorite suite (148–145 Ma)

Samples from the post-kinematic suite include a strongly porphyritic dacite sheet (09DBO13), a biotite–hornblende tonalite from the Ragged Creek pluton (08DBOJ13), a biotite–hornblende tonalite from the Dixie Creek pluton (07DBO24), and a biotite–hornblende tonalite from the Dixie Meadows pluton (08DBOJ12) (Fig. 2). Samples from this suite yield concordant individual spot analyses, with minor xenocrystic populations of ~162–160 Ma and 156–154 Ma. The pronounced Pb-loss effects observed in the older suite are minor and/or absent in the

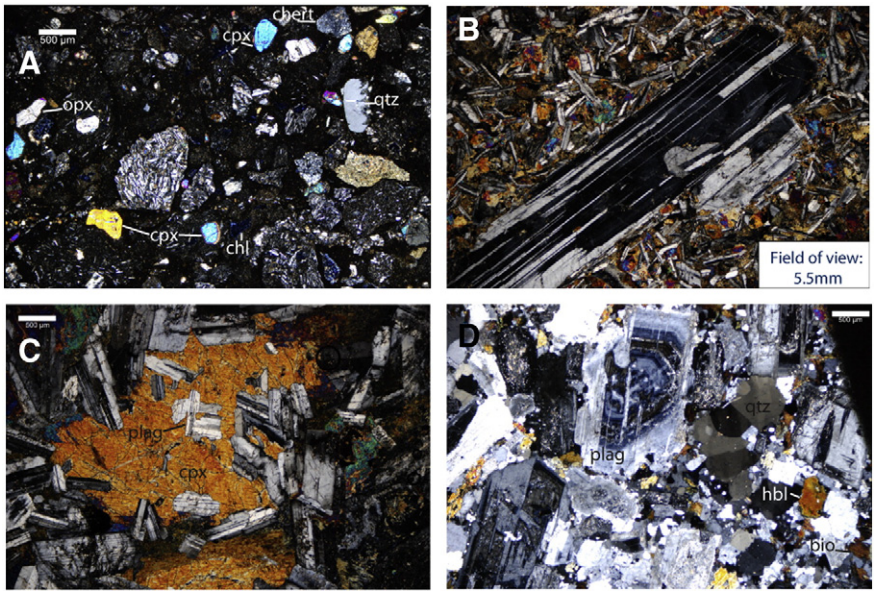

Fig. 4. Photomicrographs of metavolcanic and plutonic rocks of the Dixie Butte area. (A) Crystal lithic–clast volcaniclastic breccia contains abundant angular to subrounded trachytic basaltic andesite clasts and detrital augite and plagioclase, with minor chert, graphitic argillite, orthopyroxene, quartz, and carbonate grains; (B) Representative example of the Dixie Butte Meta-andesite flow rock displaying porphyritic texture consisting of large plagioclase phenocrysts in a fine-grained matrix of clinopyroxene and plagioclase mircolites; (C) Dixie Summit diorite (~157 Ma) displays ophitic texture with resorbed (?) plagioclase surrounded by clinopyroxene; (D) Dixie Creek biotite–hornblende tonalite (~146 Ma) has seriate texture consisting of large plagioclase feldspar and quartz with minor hornblende and biotite.

tonalite–trondhjemite–granodiorite suite. We interpret the weighted-average $^{206}Pb/^{238}U$ age of samples from this suite as follows: Wickiup Creek dacite: 148.4 ± 1.2 Ma (MSWD = 1.6) (Fig. 6E); the Ragged Creek pluton 147.0 ± 2.5 Ma (MSWD = 1.5) (Fig. 6F); the Dixie Creek pluton: 146.3 ± 1.6 Ma (MSWD = 1.8) (Fig. 6G); and the Dixie Meadows pluton: 145.0 ± 2.7 Ma (MSWD = 1.5) (Fig. 6H).

4.4. Whole rock geochemistry

4.4.1. Metavolcanic and gabbro–diorite–granodiorite suite (162–157 Ma)

Metavolcanic rocks of the Dixie Butte Meta-andesite unit are chiefly medium-K, basalts to andesites with the majority of samples plotting as basaltic andesites (DR Figs. 1–4). They range from ~50 to 57 wt.% SiO_2 and MgO concentrations range up to 9 wt.%. They are magnesian, calcic and metaluminous, and straddle the tholeiitic to calc-alkaline field (Fig. 7) (Miyashiro, 1974). Metavolcanic rocks are distinguished by low Na_2O (typically <4.0 wt.%), Sr (<400 ppm), Sr/Y (<40), La/Yb (<10), and high MgO (3–9 wt.%), CaO (6–12 wt.%), and Y (17–54 ppm) (Fig. 8). Chondrite-normalized, rare-earth-element (REE) abundance diagrams illustrate slight light-rare-earth-element (LREE) enrichment with weak positive to negative Eu anomalies (Fig. 9). Relative to normal mid-ocean-ridge basalt (N-MORB), Dixie Butte Meta-andesites display large ion lithophile element (LILE) enrichment with prominent positive K, Pb and Sr anomalies, negative Nb anomalies, and flat to slightly enriched high field strength element patterns (Fig. 10). Ce/Y values for basalts (<54 wt.% SiO_2: c.f., Mantle and Collins, 2008) range from 0.68 to 1.1, and are consistent with a maximum crustal thickness of 23 km.

Dixie Summit and Equity plutonic rocks are also magnesian, calcic and metaluminous (Fig. 7). They range from ~51 to 60 wt.% SiO_2. They display low K_2O (typically <1.1 wt.%), Sr (<400 ppm), Sr/Y (<40), La/Yb (<10), and high Al_2O_3 (16–21 wt.%), CaO (4–12 wt.%), and Y (18–56 ppm) (Fig. 8). Chondrite-normalized, REE abundance diagrams display slight LREE enrichment, and both positive and negative Eu anomalies (Fig. 9). Relative to N-MORB, Dixie Summit and Equity plutonic rocks are similar to Dixie Butte Meta-andesites and display LILE enrichment with prominent positive K, Pb and Sr anomalies, strongly negative Nb anomalies, and flat to slightly enriched high field strength element patterns (Fig. 10). Ce/Y values for gabbros (<54 wt.% SiO_2) range from 0.57 to 0.73, which are consistent with a maximum crustal thickness of ~16 km.

Standard Creek granodiorites are ferroan to magnesian, metaluminous, and alkali-calcic to calc-alkalic (Fig. 7). They range from ~64 to 68 wt.% SiO_2. They have low Sr (<400 ppm), Sr/Y (<40), La/Yb (<10), and high K_2O (>2.0 wt.%), Na_2O (>5.0 wt.%), and Y (27–58 ppm) (Fig. 8). Chondrite-normalized, REE abundance diagrams display LREE enrichment, flat heavy-REE abundances and negative Eu anomalies (Fig. 9). Relative to N-MORB, Standard Creek granodiorites display LILE enrichment with prominent a positive Pb anomaly and strong negative Nb, Sr, P and Ti anomalies (Fig. 10).

4.4.2. Tonalite–trondhjemite–granodiorite suite (148–145 Ma)

Younger tonalites and subvolcanic dacite porphyries (148–145 Ma: see below) in the western portion of the Dixie Butte area range from 54 to 67 wt.% SiO_2 (Fig. 7). They are magnesian, calcic to calc-alkalic, and metaluminous (Fig. 7). They display steeply fractionated REE abundance patterns (Fig. 9), lack Eu anomalies, and have elevated Sr concentrations (>600 ppm), La/Yb (>10) and Sr/Y values (>40) (Fig. 8). Relative to N-MORB, tonalites and dacites display LILE enrichment with prominent positive K, Pb and Sr anomalies, and negative Nb anomalies (Fig. 10).

4.5. Zircon Hf isotope data

Lu–Hf isotopic data were collected to evaluate potential sources of plutonic rocks in the Dixie Butte area and possible changes through time. From oldest to youngest, weighted average initial epsilon Hf values (2σ) are: 12.3 ± 1.2 (MSWD = 0.9) for Dixie Summit pluton; 11.3 ± 1.6 (MSWD = 0.3) for the Equity pluton; 10.1 ± 1.0 (MSWD = 1.1) for the Standard Creek pluton; 10.5 ± 1.6 (MSWD = 0.5) for the Wickiup Creek dacites; and 7.8 ± 1.9 (MSWD = 0.6) for the Dixie Creek pluton (Fig. 11). The Dixie Creek pluton displays the broadest range in initial $^{176}Hf/^{177}Hf$ values and a slightly lower weighted average value that may indicate assimilation of an evolved crustal source (e.g., Badger Creek sedimentary unit: Schwartz et al., 2011). Whereas initial epsilon Hf isotopic values show little change, $^{176}Lu/^{177}Hf$ isotopic values show a dramatic shift to lower values through time (Fig. 11), consistent with whole rock trace

Fig. 5. Cathodoluminescence images of zircons from the Dixie Butte area. Scale bars are 100 microns.

element data indicating low HREE concentrations in the 148–145 Ma, high Sr/Y plutons relative to the 162–157 Ma, low Sr/Y rocks.

5. Discussion

5.1. Geochemical modeling of high Sr/Y magmas

Siliceous magmas having high Sr/Y values and HREE-depleted chondrite-normalized REE abundances can be generated by a number of processes, including fractional crystallization of mafic, mantle-derived magma (Alonso-Perez et al., 2009; Macpherson et al., 2006; Rooney et al., 2011), magma mixing (Guo et al., 2007a, 2007b), and partial melting of garnet-bearing metabasaltic rocks (Drummond and Defant, 1990; Johnson et al., 1997; Martin, 1987). The common denominator in all of these scenarios is that high Sr/Y magmas are generated at high pressures, within the stability field of garnet (c.f., Moyen, 2009).

In this section, we investigate the origin of the high Sr/Y and HREE-depleted characteristics of the post-kinematic plutons from the Dixie Butte area. We focus particularly on the Dixie Creek pluton, from which we have the most complete sample coverage; however, in light of compositional similarities, conclusions drawn here can be applied to other post-kinematic plutons, from which fewer samples were

collected. Mineral–liquid partition coefficients used in the trace element calculations are given in DR Table 6.

5.1.1. Fractional crystallization

Major element mass balance calculations (Bryan et al., 1969) were performed using mafic magmatic enclaves from the Dixie Creek pluton and the Wickiup Creek dacite as a parental composition. These enclaves are similar to enclaves in plutons elsewhere in the Greenhorn subterrane (e.g., Johnson et al., 2007; Johnson, unpublished results), and therefore probably represent the predominant mantle-derived component in this area during Late Jurassic time. In some calculations, we also used the most mafic main-stage rock from the Dixie Creek

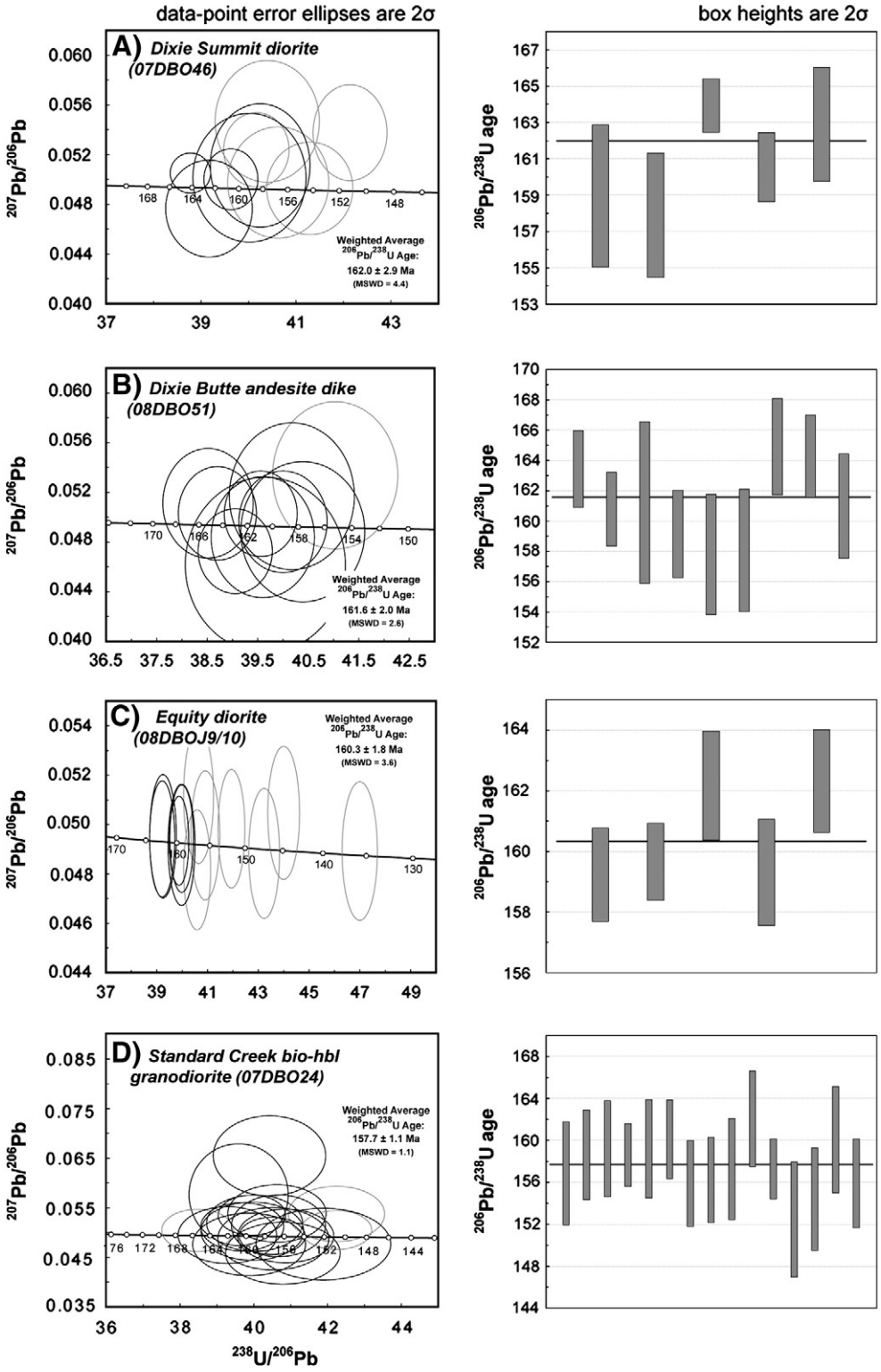

Fig. 6. Tera-Wasserburg diagrams for plutonic and volcanic rocks in the Dixie Butte area. Error ellipses and calculated ages are given at 95% confidence level. Data shown in A–E, G were collected by ion microprobe at the Stanford-USGS SHRIMP facility, whereas data shown in F and H were collected by LA-MC-ICPMS at the University of Arizona LaserChron Laboratory.

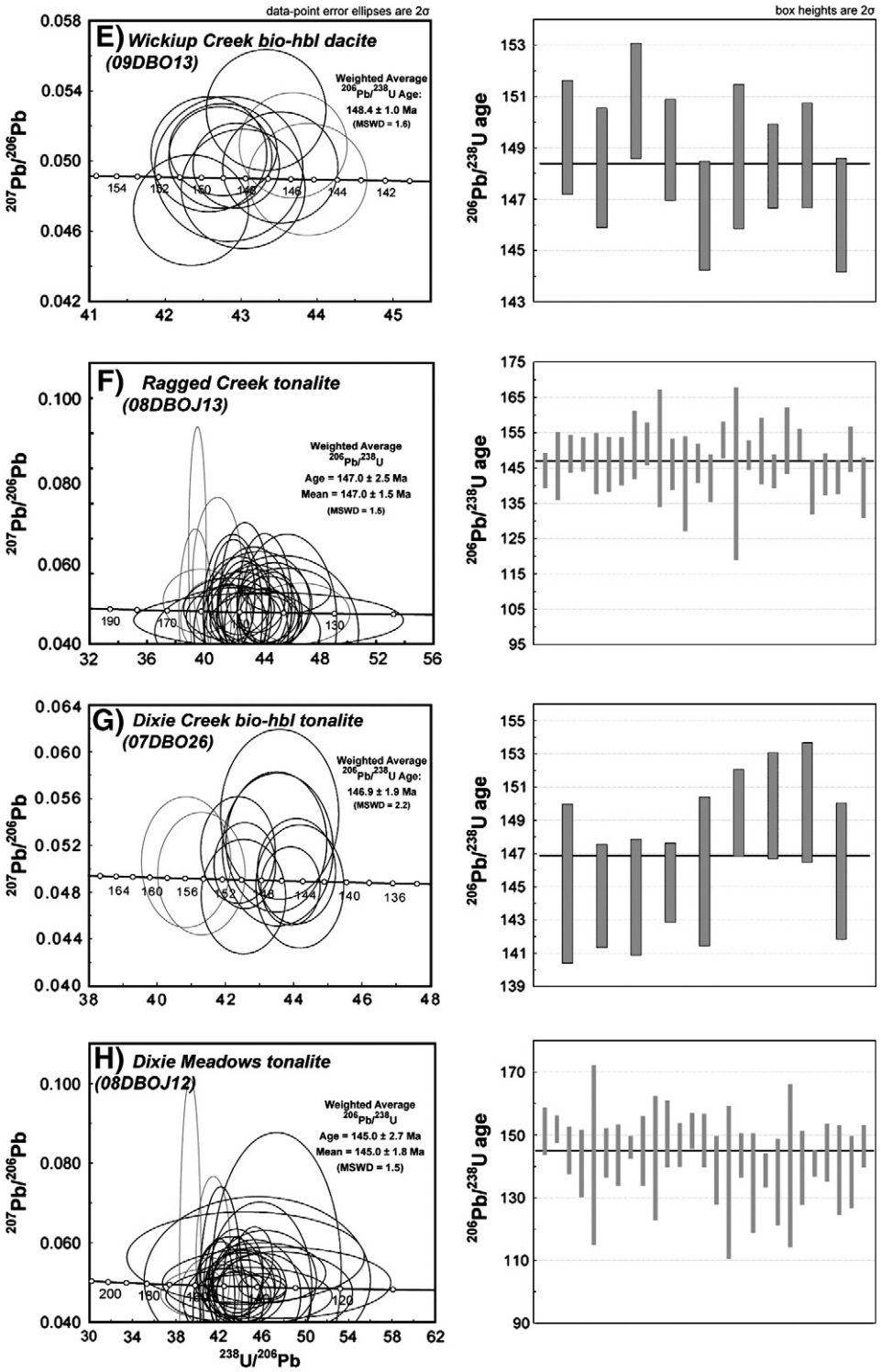

Fig. 6 (*continued*).

pluton (sample 08DBO16) as a possible parental composition. Although garnet is not present in these rocks, we included garnet compositions from Alonso-Perez et al. (2009) in some fractional crystallization calculations to determine if it played a role in the genesis of the high Sr/Y signature of the more felsic rocks. A sum of the squares of the residuals less than unity (ssr<1) was considered acceptable, and the results of those calculations were further tested with trace elements. A summary of results of the mass balance calculations are shown in DR Table 7.

None of the high-pressure mineral assemblages (garnet + hornblende ± plagioclase [$An_{43–47}$] ± magnetite ± apatite ± sphene) is compatible with the evolution of either the enclave magma or sample 08DBO16 to the most siliceous Dixie Creek sample by fractional crystallization (Models 1A–1D). Furthermore, fractionation of a low-pressure assemblage (plagioclase [$An_{43–47}$] + hornblende ± biotite ± magnetite ± apatite ± sphene) did not produce acceptable results using an enclave composition as the parental magma (Model 2A; DR Table 7). The only acceptable results were produced using sample 08DBO16, by removal of a low

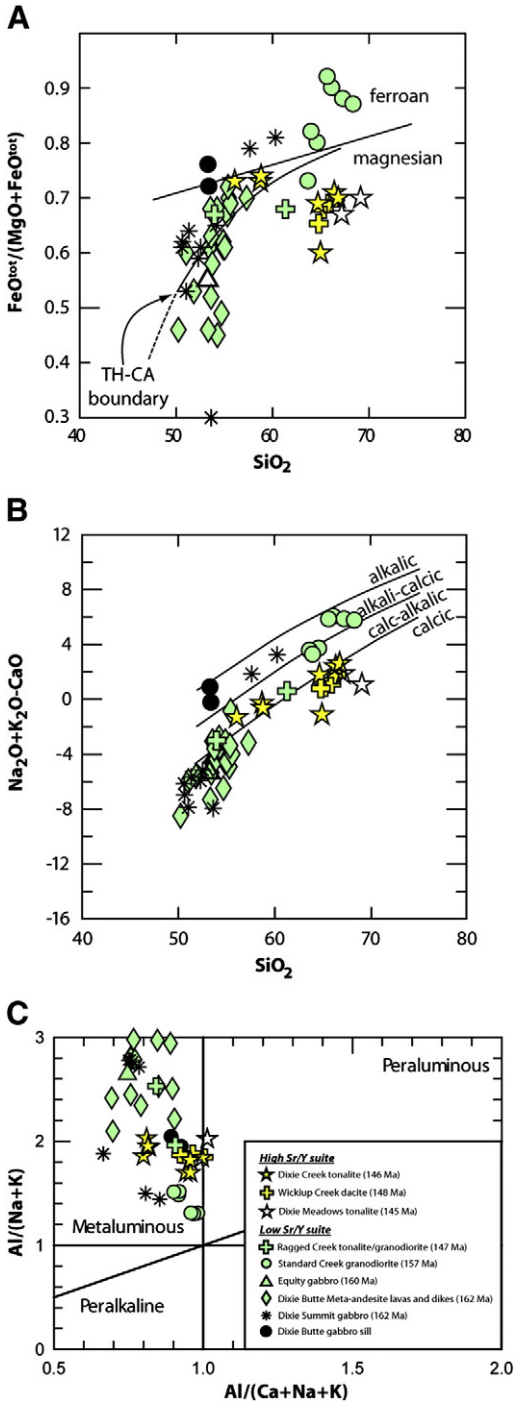

Fig. 7. Major element geochemical plots for plutonic and volcanic rocks in the Dixie Butte area. (A) $FeO^{tot}/(FeO^{tot}+MgO)$ versus weight percent SiO_2. (B) Plot of Na_2O+K_2O–CaO versus SiO_2. (C) Alumina saturation indices indicating the metaluminous to peraluminous character of the plutonic rocks in the Dixie Butte area.

pressure assemblage of plagioclase ($An_{43–47}$) + hornblende + magnetite ± apatite ± sphene (Models 2B, 2C). However, trace element calculations using the results of Model 2C cannot reproduce the high Sr/Y values of the more felsic Dixie Creek rocks (Fig. 12A). Removal of the assemblage in Model 2C will drive the residual magma composition to lower Y abundances and Sr/Y values. Furthermore, fractionation of magnesio-hornblende will result in a residual liquid (e.g., sample 08DBO9) with lower Mg#, unlike the trend observed in Fig. 8. Wallrocks at the level of emplacement (Badger Creek metasedimentary unit and Dixie Butte Meta-andesite) have low Sr/Y values; therefore, assimilation of these rocks cannot account for the high Sr/Y values of the Dixie Creek pluton (Fig. 12A). Thus, we conclude that the high Sr/Y siliceous rocks in the Dixie Creek pluton were not produced by fractional crystallization of a more mafic magma.

5.1.2. Magma mixing

The low Mg# of the least siliceous main stage rocks of the Dixie Creek pluton, relative to the more felsic rocks, suggests they are not related by fractional crystallization (see above), either as the parental magma or as a hornblende-rich cumulate. Therefore, these rocks (e.g., sample 08DBO16) likely represent the intrusion of a separate magma that mixed incompletely with the more felsic magma (e.g., sample 08DBO9; see Guo et al., 2007a, 2007b).

Main stage rocks from the Dixie Creek pluton also have a bimodal distribution; the more mafic rocks have SiO_2 contents between 56 and 59 wt.% and lower average Sr/Y values, whereas the felsic rocks range from 65 to 67 wt.% and have higher average Sr/Y values. With one exception (sample 08DBO57), the Dixie Creek samples plot along a mixing line between samples 08DBO16 (~56 wt.% SiO_2) and 08DBO9 (~67 wt.% SiO_2) for most elements (Fig. 12B). Although not definitive, a magma mixing origin is consistent with some of the compositional trends observed in the Dixie Creek rocks and suggests that coeval high and low Sr/Y magmas were present during the magmatic construction of the Dixie Creek pluton.

5.1.3. Partial melting

Partial melting calculations were performed using the equation for batch partial melting. Although the subsurface geology of the Dixie Butte area is not known, we simulated partial melting of various mafic rock types in the Greenhorn subterrane (Schwartz et al., 2011), using average compositions for: 1) plutonic (gabbro and diorite) and volcanic (keratophyre) rocks from the Canyon Mountain complex (south of Dixie Butte), 2) basalts and gabbros from the Vinegar Hill region (north of Dixie Butte), 3) Dixie Butte Meta-andesite, and 4) pillow lavas from Olive Creek (from the Bourne subterrane northeast of Dixie Butte). All the models assume that the high Sr/Y rocks represent liquid compositions.

Results of the trace element calculations allow us to make some general conclusions: 1) None of the models allows for residual plagioclase, which is consistent with the high Sr/Y values and the lack of Eu-anomalies in the Dixie Creek rocks, 2) the models require garnet in the residue, which is suggested by the low HREE and Y abundances in the felsic rocks, and 3) the results are inconsistent with a LREE-depleted source (e.g., mafic rocks from Vinegar Hill and the Canyon Mountain complex). The results most consistent with the observed REE and Sr–Y variations require a slightly LREE-enriched source, similar to mafic rocks of the Dixie Butte Meta-andesite or pillow lavas from Olive Creek unit.

Partial melting results suggest that the most felsic Dixie Creek compositions resulted from 20 to 40% melting of metabasaltic rocks in equilibrium with a residual assemblage of hornblende + garnet + clinopyroxene + trace sphene (Fig. 13). The residual mineralogy is similar to those produced in high-pressure (>10 kbar) melting experiments on basaltic compositions (Rapp et al., 1991; Rushmer, 1991; Winther and Newton, 1991; Wolf and Wyllie, 1993, 1994) and in petrologic models for other plutons in the BMP (Johnson et al., 1997, 2007). Therefore, we conclude that the high Sr/Y rocks in the Dixie Butte area are most consistent with partial melting of deep metabasaltic crust (>35 km) during Late Jurassic time.

5.2. Middle to early Late Jurassic, low Sr/Y magmatism in Dixie Butte area

Results from our geochemical, isotopic and geochronological study of the Dixie Butte area allow us to investigate the mechanisms, sources and timescales of low and high Sr/Y magma generation, and

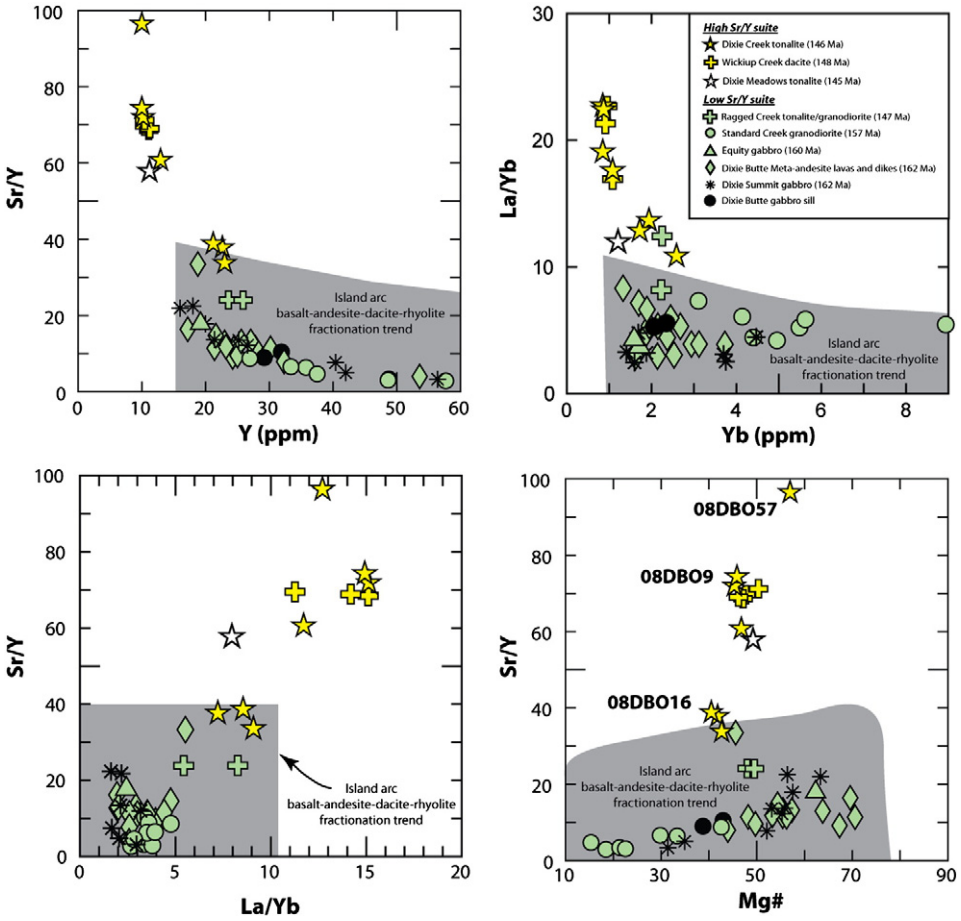

Fig. 8. Selected trace element variation diagrams. Plutonic and subvolcanic rocks of the 148–145 Ma suite display higher average La/Yb and Sr/Y versus the older 162–157 Ma suite in the Dixie Butte area. Fields for island arc basalt–andesite–dacite–rhyolite differentiation trends are shown (after Drummond and Defant, 1990). Mg# is calculated as 100 × molar MgO/(MgO + FeO^{tot}).

the relationship between high Sr/Y magmatism and widespread Late Jurassic contractional deformation (arc–arc collision) in the BMP. Our data indicate that pre- to syn-kinematic, low Sr/Y magmatism occurred from 162 to 157 Ma, and involved the emplacement of lavas, dikes and plutons into pre-existing, Permo-Triassic arc crust. Plutonism in the broader Greenhorn subterrane continued to 154 Ma indicating that this phase of magmatism spanned approximately 8 myr from ca. 162 to 154 Ma (Fig. 3; Schwartz et al., 2011). Plutons related to this phase of magmatism are bimodal with mafic (gabbro–diorite) plutons primarily restricted to the Dixie Butte area, and more felsic tonalites and granodiorites occurring both in the Dixie Butte area (e.g., Standard Creek pluton) and to the northeast in the Greenhorn subterrane of the Baker terrane. Both mafic and felsic plutonic rocks display LILE enrichment, negative Nb anomalies, low Sr/Y values, and strongly positive initial epsilon Hf values indicative of hydrous partial melting of depleted-mantle peridotite or mafic arc crust (Fig. 10). Trace element discrimination diagrams for these mafic rocks support generation in a supra-subduction zone environment (DR Fig. 3), or from previously enriched hydrous mantle by supra-subduction zone-derived fluids. Similar-age (162–154 Ma) plutons to those observed in the Greenhorn subterrane also occur in the Wallowa terrane (c.f., Unruh et al., 2008).

Low Sr/Y magmatism in the Dixie Butte area is partially coeval with widespread Late Jurassic thrusting and folding in the BMP interpreted to signify terminal collision of the Wallowa and Olds Ferry island arcs (Avé Lallemant, 1995; Schwartz et al., 2010, 2011). Late Jurassic deformation involved folding and faulting (thrusting) at terrane (e.g., Wallowa–Baker) and subterrane (e.g., Greenhorn–Bourne) boundaries. In the Baker terrane, deformation at the Bourne–Greenhorn subterrane boundary involved thrusting of the Greenhorn subterrane over the Bourne subterrane, intense brecciation in footwall chert argillite and localized cataclastic shearing associated with greenschist-facies metamorphic veining in both hanging-wall and footwall rocks (Evans, 1995; Schwartz et al., 2011). The effects of Late Jurassic deformation in the Dixie Butte area are not as intense as near terrane and subterrane boundaries; however, early low Sr/Y plutonic and volcanic rocks display pervasive propyllitic alteration and folding of basal volcanogenic sedimentary rocks which may be related to Late Jurassic contractional deformation. These alteration features are not observed in the younger, high Sr/Y suite (148–145 Ma) suggesting that deformation and regional greenschist-facies metamorphism/alteration had ceased by ca. 148 Ma.

Our preferred model for the evolution of the Dixie Butte area and the broader Blue Mountains province is depicted in the top two panels of Fig. 14 (after Schwartz et al., 2011). In this model, a doubly vergent subduction system similar to that of the present-day Molluca sea resulted in mantle-derived, low Sr/Y magmatism in both the Wallowa (Lee, 2004; Unruh et al., 2008) and Dixie Butte area. Closure of this doubly vergent subduction system generated north- and south-dipping thrust and reverse faults at opposing ends of the Baker terrane (c.f., Fig. 1 and cross-section). Although our ages are restricted to ca. 162–157 Ma in the Dixie Butte area, mafic magmatism in the Baker/Izee area likely began as early as Early to Middle Jurassic based on volcaniclastic sedimentary rocks and associated andesitic lavas, dikes and sills in the John Day region (c.f., Dickinson and Thayer, 1978; Dickinson and Vigrass, 1965; Dorsey and LaMaskin, 2007). Paleocurrent indicators and thickness relations indicate a northerly source for

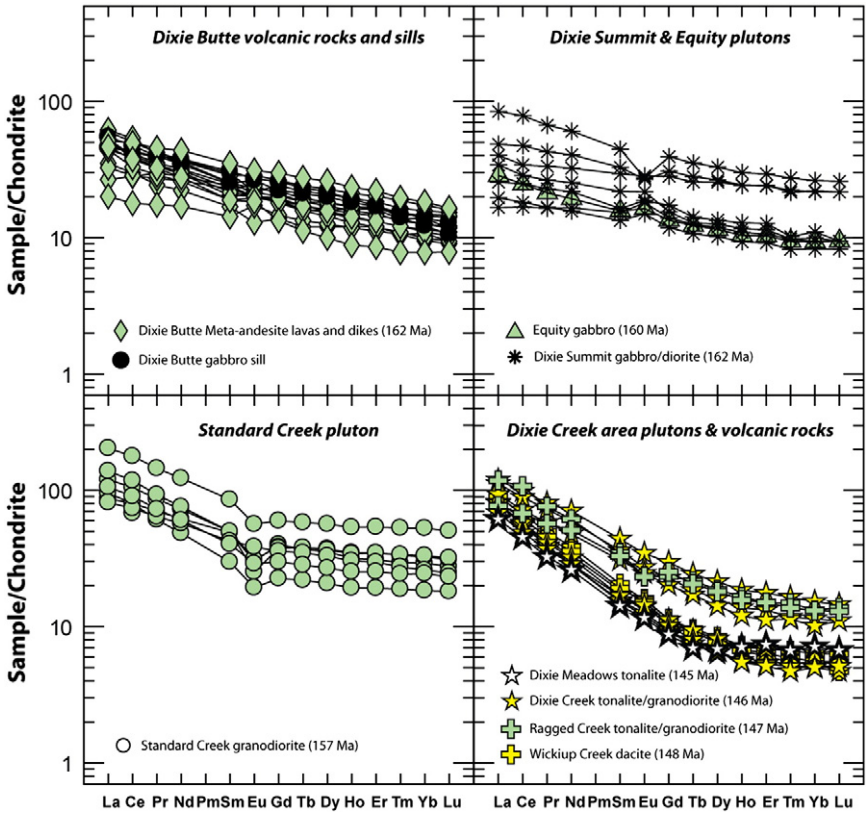

Fig. 9. Chondrite-normalized rare-earth-element abundance diagrams for igneous rocks of the Dixie Butte area. Samples are normalized to chondrite values of Sun and McDonough (1989).

these volcaniclastic rocks, consistent with the location of voluminous mafic magmatism in the Dixie Butte area (Dickinson and Thayer, 1978). Magmatism terminated during the waning stages of arc–arc collision and transitioned in character from dominantly magnesian, calcic to calc-alkalic (e.g., Dixie Butte Meta-andesites, Dixie Summit and Equity plutons) to more ferroan and alkali-calcic varieties (e.g.,

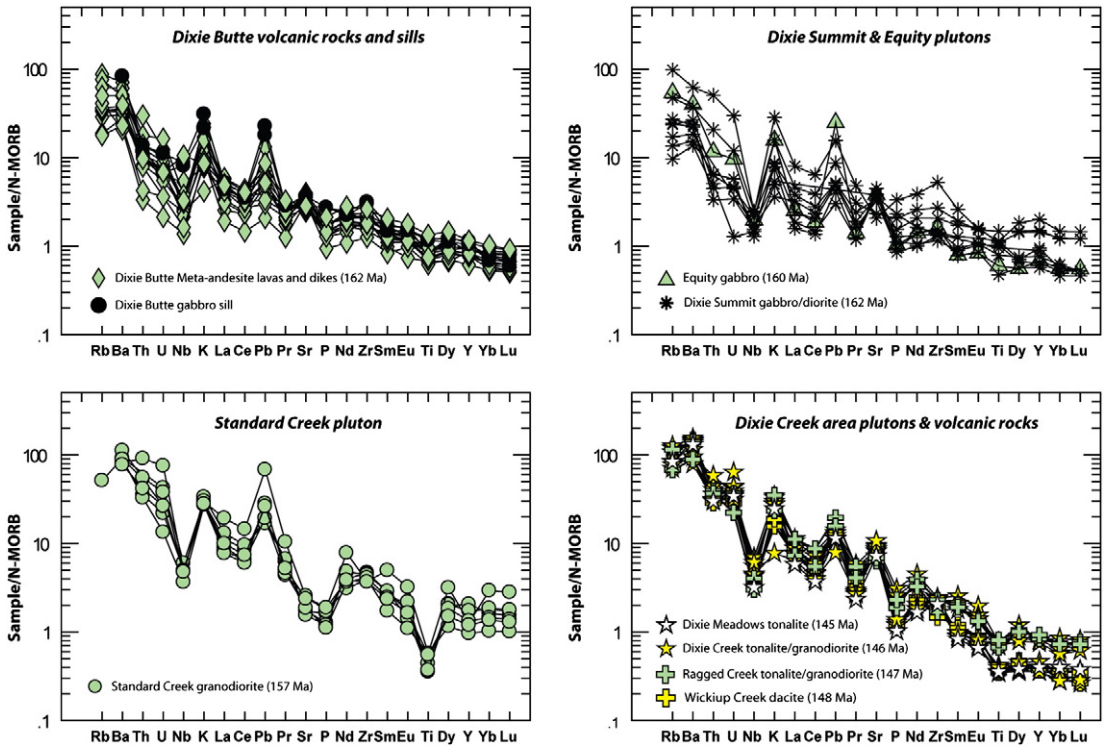

Fig. 10. N-MORB normalized trace element abundance diagrams for igneous rocks of the Dixie Butte area. Samples are normalized to N-MORB values of Sun and McDonough (1989).

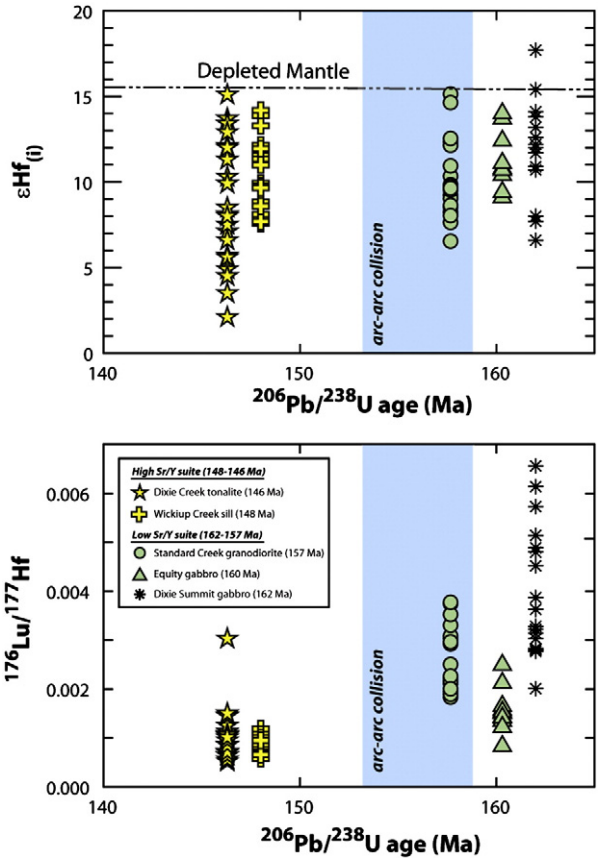

Fig. 11. Zircon Lu–Hf isotopic data for low Sr/Y and high Sr/Y suites. Initial Hf values are calculated at the time of crystallization using calculated weighted average $^{206}Pb/^{238}U$ ages (this study). Both low and high Sr/Y suites show similar strongly positive initial Hf isotopic values; however, $^{176}Lu/^{177}Hf$ values are consistently lower in the high Sr/Y rocks likely due to the presence of garnet in the residue.

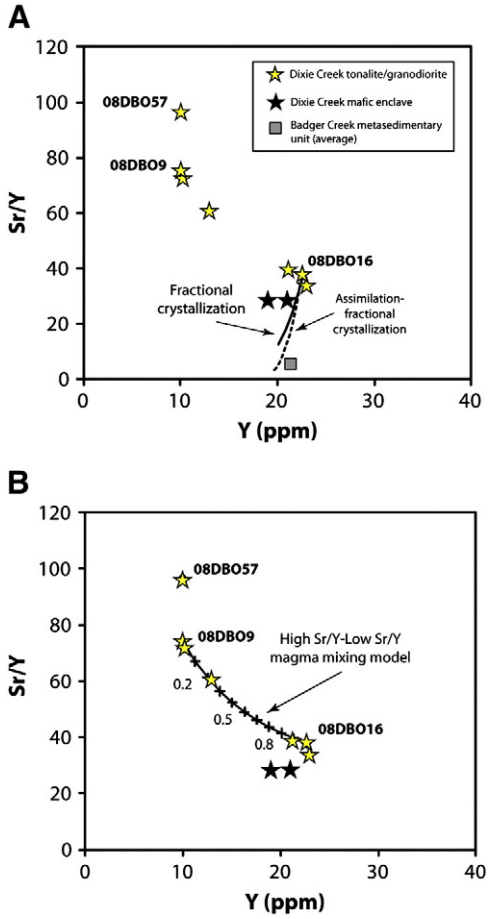

Fig. 12. (A) Results of fractional crystallization (FC) and assimilation-fractional crystallization (AFC) calculations. Yellow stars are main stage samples from the Dixie Creek pluton, black stars represent magmatic enclaves, and gray square symbol represents the wallrock composition at the depth of emplacement (average Badger Creek metasedimentary rock composition). (B) Results of magma mixing calculations between high Sr/Y and lower Sr/Y endmembers. Numbers beside the mixing curve indicate the weight fraction (F) of the mafic end member in the mixture.

Standard Creek pluton: 157 Ma). This transition may reflect derivation from reduced basaltic magmas either by fractional crystallization or partial melting as subduction ceased.

5.3. Late Jurassic, post-collisional magmatic lull and temporal transitions from low Sr/Y to high Sr/Y magmatism

Widespread Late Jurassic contractional deformation in the BMP (159–154 Ma) was followed by a magmatic lull from ca. 154 to 148 Ma. Post-kinematic, high Sr/Y magmatism in the Dixie Butte area initiated at 148 Ma (~6 myr following cessation of Late Jurassic regional contraction) and spanned a brief, ~3 myr interval from 148 to 145 Ma. Magmatic rocks related to this event in the Dixie Butte area are bimodal displaying both high and low Sr/Y values. Best-fit partial melting models for the high Sr/Y magmas suggest they formed from ~20–40% hydrous partial melting of a LREE-enriched source (e.g., Dixie Butte Meta-andesites or Olive Creek basalts: Fig. 13). The role of fluids during partial melting is not well constrained; however, hydrous partial melting conditions are plausible given the presence of amphibole and the lack of plagioclase in our predicted partial melting residue (Fig. 13). Xenocrystic zircon populations in the high Sr/Y magmas (c.f., 162–160 and 156–154 Ma populations: Fig. 5) also support partial melting of a meta-andesite source, and/or later assimilation during magma ascent.

Our geochemical results suggest that post-collisional high Sr/Y magmas were produced from hydrous partial melting of LREE-enriched crust in the garnet stability field; however, the heat source necessary to partially melt the source region shortly after contractional deformation is poorly constrained. Advection of heat (e.g., mafic underplating) is likely necessary since burial of crust over such short timescales (~6 myr) is unlikely to produce temperatures required for partial melting. Mafic enclaves in the high Sr/Y rocks (e.g., Dixie Creek pluton, the Wickiup Creek dacites), and ca. 148 Ma mafic plutonic rocks in the nearby Sunrise Butte composite pluton imply that mafic magmas were spatially and temporally associated with high Sr/Y magmatism in the region (Fig. 1).

One possible mechanism for the generation of mafic magmas in the Dixie Butte area is the initiation of renewed subduction beginning at 148 Ma. In the adjacent Bourne subterrane, voluminous low Sr/Y magmatism occurred from ca. 148 to 141 Ma (Fig. 1) and consisted of tonalite and granodiorite plutons and batholiths (e.g., Bald Mountain and Wallowa batholiths). Although the Late Jurassic geodynamic setting of the BMP is not well constrained, previous workers have interpreted these rocks as having formed in a supra-subduction zone setting from partial melting of shallow mafic arc crust and/or depleted mantle (c.f., Johnson and Schwartz, 2009; Taubeneck, 1995). We speculate that the high Sr/Y magmatic activity that we observe in the Greenhorn subterrane may have been triggered by mafic underplating of basaltic magmas produced during this short-lived phase (~7 myr) of renewed subduction-related magmatism (Fig. 14). In this model, Late Jurassic magmatism in the BMP (148–141 Ma) occurred as the result of west-dipping subduction beneath the Olds Ferry island arc. Subduction

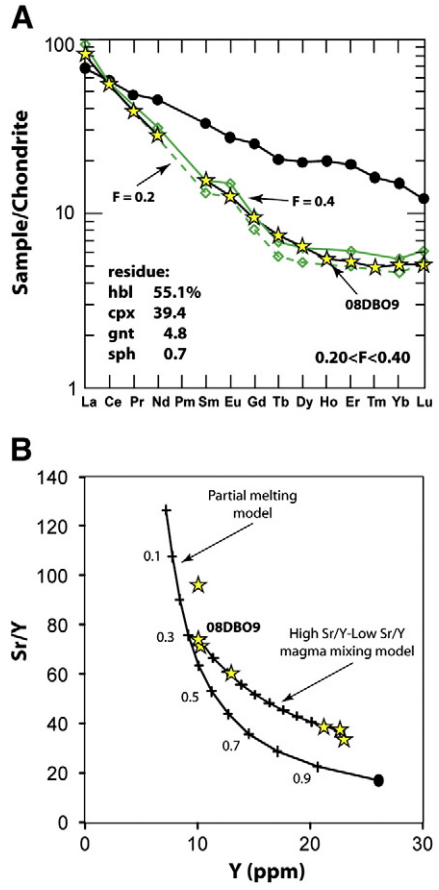

Fig. 13. Results of partial melting calculations. (A) Chondrite-normalized REE abundance diagram (normalization values of Sun and McDonough, 1989). F, weight fraction of melt produced. The open diamond symbol with the dashed line and the open diamond with the solid line represent the melt compositions at F = 0.2 and F = 0.4, respectively. Yellow stars represents sample 08DBO9 (felsic, high Sr/Y), and the pattern with the solid black circle represents the LREE-enriched metabasaltic source composition (average Olive Creek pillow basalt; Schwartz et al., in press). (B) Diagram of Sr/Y versus Y. The source composition (filled circle) is the same as in (A). Yellow stars represent samples from the Dixie Creek pluton. Numbers beside curve represent melt fractions. Note that sample 08DBO9 is consistent with approximately 30–35% melting, in agreement with the REE results (A). Magma mixing model from Fig. 12 is shown for reference.

resulted in tectonic closure of the back-arc basin (Salmon River suture zone: e.g., Gray and Oldow, 2005) separating North America and the amalgamated terranes of the BMP. Early Cretaceous deformation and metamorphism in this region is indicated by ca. 144 Ma Sm–Nd garnet-whole rock isochron data from the Pollock Mountain plate (Salmon River suture zone: Getty et al., 1993). Dehydration partial melting of the mantle wedge, and mafic underplating beneath the Baker terrane associated with closure of the Salmon River suture zone may explain the temporal association of both voluminous low Sr/Y magmatism in the Baker and Wallowa terranes, and bimodal high and low Sr/Y magmatism in the Dixie Butte area.

An alternative interpretation for the high Sr/Y signatures in the 148–145 Ma suite is that they formed from partial melting of subducting oceanic crust, rather than partial melting of lower crust. Magmas generated by slab melting are commonly andesitic to dacitic in composition (e.g., high Mg# andesites: Yogodzinski and Kelemen, 1998), have high Sr/Y (>100), high Cr (>36 ppm), Ni (>24), Mg# (40–70) and Al_2O_3 (>15 wt.%), and steeply fractionated REE patterns suggestive of an eclogitic residue. Typically, slab-derived melts occur from partial melting of young (<5–10 Ma: Peacock: 1994) actively subducting oceanic crust whereby high Cr, Ni and Mg# values reflect interaction with the overlying mantle wedge. In contrast to slab melts in modern subduction zones (e.g., Drummond and Defant, 1990), high Sr/Y tonalites and dacites in the Dixie Butte area display low Cr (<22 ppm), Ni (<10 ppm) and Mg# (<55). A number of other features are also difficult to reconcile with a slab melting model, including: 1) the spatial restriction of the high Sr/Y rocks to the Greenhorn subterrane, 2) the temporal transition from low Sr/Y to high Sr/Y in the Dixie Butte area following regional contraction, and 3) the spatial association with a coeval belt of low Sr/Y plutons and batholiths in the nearby Bourne subterrane. In modern settings, island arc crust is rarely sufficiently thick for garnet to exist as a stable residual phase during lower crustal partial melting; however, in the BMP, Late Jurassic arc–arc collision provides a mechanism for producing requisite crustal thickening necessary for the generation of high Sr/Y in a supra-subduction zone environment.

The transition from low to high Sr/Y magmatism following arc–arc collision also has implications for crustal thickness variations through time. Whereas Ce/Y values for basalts and gabbros of the low Sr/Y suite are consistent with maximum crustal thickness of ~23 km at ca. 160 Ma (Mantle and Collins, 2008), geochemical evidence for garnet as a residual phase in equilibrium with high Sr/Y melts suggests a minimum crustal thickness ≥35 km at 148 Ma. These results imply that the crust in the Dixie Butte area was thickened by at least 12 km or more, corresponding to ~34% shortening as a result of Late Jurassic contractional deformation.

5.4. High Sr/Y plutonism in the western North American Cordillera following arc–arc and arc–continent collisions

The occurrence of high Sr/Y magmas following widespread regional contraction in the BMP raises a number of questions regarding the generation of high Sr/Y magmas in evolving orogenic belts, and the significance of high Sr/Y magmatism during tectonic accretion of arc-related rocks along the western North American Cordillera in the Phanerozoic. For example, how common are high Sr/Y plutons in other areas of the western North American Cordillera (e.g., Klamath Mountains, Sierra Nevadas, Peninsular Ranges, Salmon River suture zone) and to what extent is their generation influenced temporally and spatially by collisional processes? More specifically, are high Sr/Y magmas common features following Late Jurassic to Early Cretaceous orogenesis and to what degree are tectonic and magmatic events in the BMP geodynamically linked to other regions (e.g., Klamath and Sierra Nevada, Northwest Nevada)? Below we briefly discuss other high Sr/Y plutonic belts in the western North American Cordillera whose generation are also linked to major contractional events.

Southwest of the Blue Mountains province, plutonic rocks in the Klamath Mountains record a similar tectono-magmatic history of early low Sr/Y magmatism, contractional deformation and subsequent post-kinematic, high Sr/Y magmatism in the Late Jurassic. In this region, a suite of high Sr/Y plutons (ca. 148–144 Ma) post-date Late Jurassic regional contraction (Nevadan orogeny) at 153–150 Ma (e.g., Allen and Barnes, 2006; Chamberlain et al., 2006; Harper and Wright, 1984; Harper et al., 1994; Saleeby et al., 1982). These post-kinematic, high Sr/Y plutons comprise the latest phase of the ca. 151–144 Ma "western Klamath plutonic suite" which consists of early low Sr/Y, pre- to syn-kinematic mafic plutonic rocks (chiefly gabbro–diorite), followed by late-stage, high Sr/Y tonalites and granodiorites (Barnes et al., 1996, 2006). High Sr/Y plutons include the Pony Peak (144.2 ± 2.5 Ma: Allen and Barnes, 2006), Bear Peak (143.7 ± 1.3 Ma: Allen and Barnes, 2006) and late-stage phases of the Bear Mountain intrusive complex (ca. 148–147 Ma: Chamberlain et al., 2006), the latter of which intrudes the Late Jurassic Orleans (Preston Peak) thrust fault (Snoke, 1977; Snoke et al., 1981). All high Sr/Y plutons bear a number of similarities to coeval high Sr/Y magmatic rocks in the BMP including high Na_2O (>5.0 wt.%), 2), Sr (>600 ppm), Sr/Y (>40) and La/Yb (>10) values, and low Y

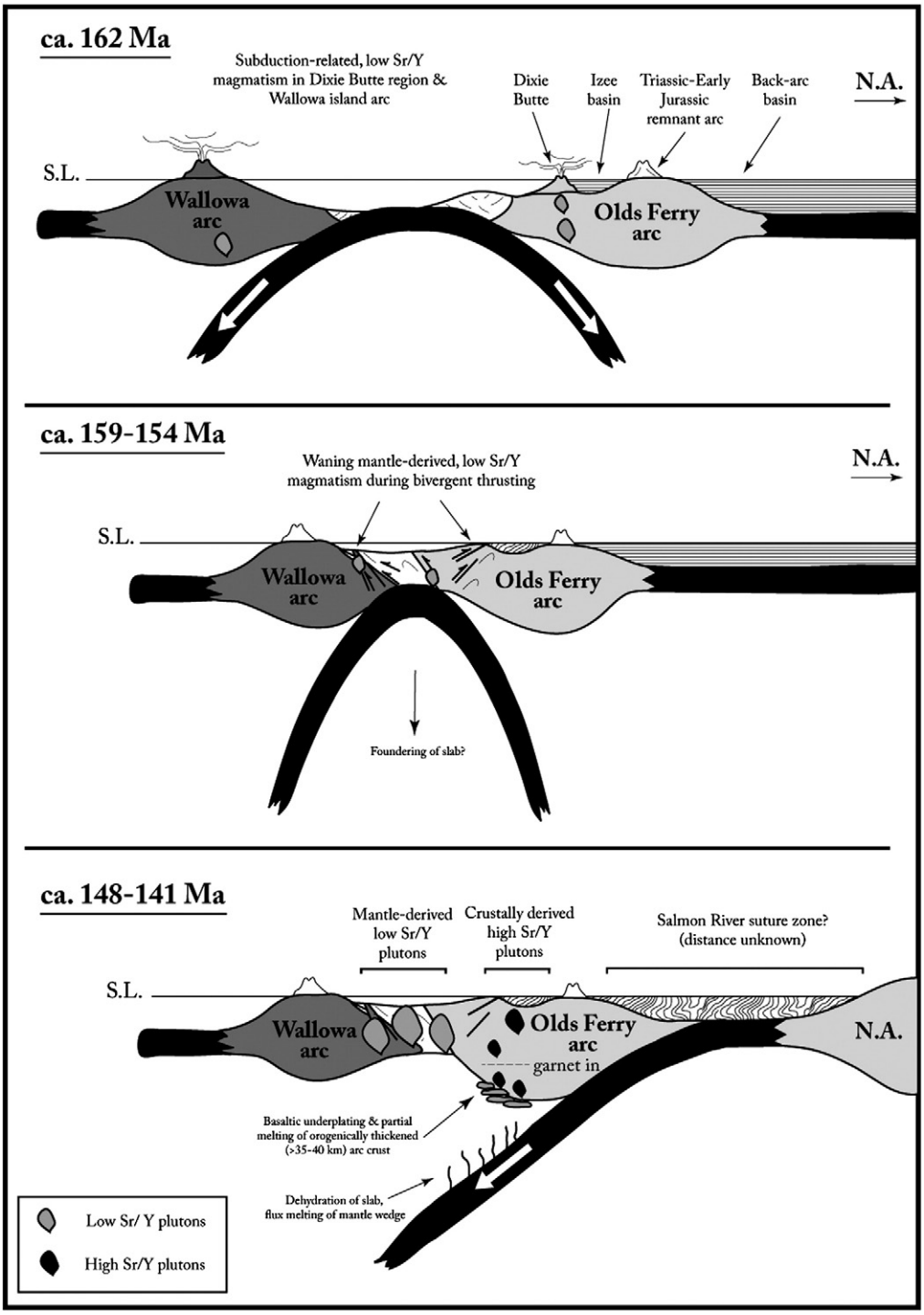

Fig. 14. Schematic, pre- (ca. 162 Ma), syn- (159–154 Ma), and post-collisional scenarios for the generation of low and high Sr/Y suites in the Blue Mountains province (not to scale). Following regional contraction at 159–154 Ma, high Sr/Y plutons formed in the orogenically thickened region of the Greenhorn subterrane (interpreted to be the forearc of the Olds Ferry island arc system) perhaps due to mafic underplating from subduction-related magmas. Coeval low Sr/Y plutons in the outboard regions of the Bourne subterrane (Baker terrane) and the Wallowa island arc suggest renewed subduction at 148–141 Ma following terminal arc–arc collision, but prior to Early Cretaceous collision of the amalgamated terranes with western North America.

(<20 ppm)—features which are consistent with partial melting of mafic crust in which amphibole + garnet + clinopyroxene are residual phases (Barnes et al., 1996, 2006). Although the timing of regional contraction in the Klamath Mountains is somewhat younger (153–151 Ma versus 159–154 Ma in the Blue Mountains province), the timing of high Sr/Y magmatism following regional contraction is similar (148–145 in Blue Mountains province versus 148–144 Ma in the western Klamath plutonic suite) suggesting that Late Jurassic high Sr/Y magmatism in these two regions may be linked by similar processes.

Along the eastern border of the BMP, in the Salmon River suture zone, Early Cretaceous high and low Sr/Y plutons (122–111 Ma: Fig. 3) intrude accreted island arc crust and the western North American margin following an intense episode of Early Cretaceous regional contraction and high-pressure/temperature prograde metamorphism at 128 ± 3 Ma

(Getty et al., 1993; Lund, 1995; Selverstone et al., 1992; Snee et al., 1995). The timing of thrusting in the Salmon River suture zone is poorly dated, but was likely underway by at least 135–130 Ma (Getty et al., 1993; Selverstone et al., 1992; Snee et al., 1995). Previous workers have interpreted this event to signify collision and underthrusting of the previously amalgamated island–arc and related rocks of the BMP (Wallowa, Baker, Olds Ferry) with the western margin of North America. Post-kinematic plutons in this region display high Sr/Y geochemical characteristics, and were emplaced primarily along the 0.704–0.706 line (Armstrong et al., 1977; Fleck and Criss, 1985; Manduca, 1988; Manduca et al., 1993) and within the adjacent Wallowa terrane (e.g., Cornucopia stock: Johnson et al., 1997). The high Sr/Y plutons in the Salmon River suture zone are spatially and temporally distinct from those we report from the Late Jurassic BMP and Klamath Mountains, but are salient in that they represent a subsequent phase (122–111 Ma) of high Sr/Y magma generation following convergence and arc–continent suturing along the western margin of North America.

Finally, the Peninsular Ranges of southern and Baja California display another example of high Sr/Y magma generation following contractional deformation attributed to arc–continent collision along the western North American Cordillera (e.g., Kimbrough et al., 2001; Tulloch and Kimbrough, 2003). The 800-km-long Peninsular Ranges batholith consists of a western, low Sr/Y (130–105 Ma) and an eastern, high Sr/Y (100–92 Ma) plutonic belt both of which are separated by a ductile thrust zone that was active from 115 to 108 Ma (Johnson et al., 1999). Pre- to syn-kinematic intrusions in the older, low Sr/Y belt range from gabbro to mozogranite, are variably deformed, and have primitive, island–arc geochemical affinities. Post kinematic intrusions in the eastern belt ("La Posta suite": Silver and Chappell, 1988; Tulloch and Kimbrough, 2003; Walawender et al., 1990) consist of relatively homogeneous tonalite and granodiorite with high Sr/Y geochemical signatures (e.g., average Sr/Y = 60, Sr = 650 ppm: Tulloch and Kimbrough, 2003). These post-kinematic, high Sr/Y plutons are similar to those observed in the Salmon River suture zone, the Klamath Mountains and the BMP (this study) suggesting that contractional deformation played an important role in the generation of high Sr/Y plutons in this region and throughout the western North American Cordillera during Phanerozoic tectonic accretion events.

6. Conclusions

High Sr/Y magmatism in the Dixie Butte region post-dates an important Late Jurassic contractional event interpreted to signify the terminal tectonic collision of the Olds Ferry and Wallowa island arc terranes. These magmas were emplaced shortly after a preceding phase of low Sr/Y magmatism and record a dramatic change in the chemistry of plutons following arc–arc collision. Our data indicate the following:

1) Low Sr/Y magmatism involved the emplacement of mafic lavas, dikes, sills and plutons into the Greenhorn subterrane between ~162 and 157 Ma. Major and trace element geochemistry and strongly positive initial epsilon Hf values are indicative of hydrous partial melting of depleted-mantle peridotite or mafic arc crust in their generation.
2) Low Sr/Y magmatism was coeval with widespread Late Jurassic thrusting and folding throughout all terranes in the Blue Mountains province. Waning low Sr/Y magmatism became ferroan and alkali-calcic (Standard Creek pluton) possibly reflecting derivation from reduced magmas as subduction ceased.
3) High Sr/Y magmatism in the Dixie Butte area followed a magmatic lull (154–148 Ma) and lasted a relatively short duration from 148 to 145 Ma. High Sr/Y tonalites and dacites have major and trace element, and zircon $^{176}Hf/^{177}Hf$ values consistent with derivation from a mafic, depleted-mantle derived source with garnet + clinopyroxene + amphibole as residual phases, and an absence of plagioclase as either a residual or fractionating phase.
4) High Sr/Y magmatism in the Klamath Mountains is coeval with magmatism in the BMP, and also follows the Late Jurassic Nevadan orogeny. Similarities in timing and geochemistry suggest that Late Jurassic high Sr/Y magmatism in the BMP and Klamath Mountains may be linked with widespread orogenic thickening and partial melting following Late Jurassic contraction.
5) The relationship between high Sr/Y magmatism and arc–arc collision in the Blue Mountains is similar to regional deformational events and magmatism in the Salmon River suture zone (122–111 Ma) and in the Peninsular Ranges of southern and Baja California (100–92 Ma).

Supplementary materials related to this article can be found online at doi:10.1016/j.lithos.2011.05.005.

Acknowledgments

We wish to acknowledge discussions with Mark L. Ferns, Art Snoke, Cal Barnes, and Bill Collins. Detailed comments from Dr. Andrew Kerr (Editor-in-Chief), Dr. Mariek Schmidt and an anonymous reviewer significantly improved our manuscript. We thank Brad Ito for keeping the SHRIMP-RG working so well and efficiently. Partial financial support for this work was provided by University of Alabama start-up funds (JJS), a University of Alabama RGC grant (JJS), NSF grant EAR-0911681 (JJS), NSF grant EAR-0911735 (KJ), and a University of Houston-Downtown Organized Research Committee grant (KJ). Support for the Arizona Laser Chron Lab is provided by NSF grant EAR-0732436.

References

Ague, J.J., Brimhall, G.H., 1988. Magmatic arc asymmetry and distribution of anomalous plutonic belts in the batholiths of California: effects of assimilation, crustal thickness, and depth of crystallization. Geological Society of America Bulletin 100, 912–927.

Allen, C.M., Barnes, C.G., 2006. Ages and some cryptic sources of Mesozoic plutonic rocks in the Klamath Mountains, California and Oregon. In: Snoke, A.W., Barnes, C. G. (Eds.), Geological studies in the Klamath Mountains Province, California and Oregon: a volume in honor of William P. Irwin: Geological Society of America, 410, pp. 223–245.

Alonso-Perez, R., Müntener, O., Ulmer, P., 2009. Igneous garnet and amphibole fractionation in the roots of island arcs: experimental constraints on andesitic liquids. Contributions to Mineralogy and Petrology 157, 541–558.

Armstrong, R.L., Taubeneck, W.H., Hales, P.O., 1977. Rb–Sr and K–Ar geochronometry of Mesozoic granitic rocks and their Sr isotopic composition, Oregon, Washington, and Idaho. Geological Society of America Bulletin 88, 397–411.

Ashley, R.P., 1995. Petrology and deformation history of the Burnt River Schist and associated plutonic rocks in the Burnt River Canyon area, northeastern Oregon. In: Vallier, T.L., Brooks, H.C. (Eds.), Geology of the Blue Mountains region Oregon, Idaho and Washington; petrology and tectonic evolution of pre-Tertiary rocks of the Blue Mountains region: U.S. Geological Survey Professional Paper, 1438, pp. 457–495.

Avé Lallemant, H.G., 1995. Pre-Cretaceous tectonic evolution of the Blue Mountains Province, northeastern Oregon. In: Vallier, T.L., Brooks, H.C. (Eds.), Geology of the Blue Mountains Region of Oregon, Idaho and Washington; petrology and tectonic evolution of pre-Tertiary rocks of the Blue Mountains region: U.S. Geological Survey Professional Paper, 1438, pp. 271–304.

Baines, A.G., Cheadle, M.J., John, B.E., Grimes, C.G., Schwartz, J.J., Wooden, J.L., 2009. SHRIMP Pb/U zircon ages constrain gabbroic crustal accretion at Atlantis Bank on the ultraslow-spreading Southwest Indian Ridge. Earth and Planetary Science Letters 287, 540–550.

Barnes, C.G., Petersen, S.W., Kistler, R.W., Murray, R.W., Kays, M.A., 1996. Source and tectonic implications of tonalite–trondhjemite magmatism in the Klamath Mountains. Contributions to Mineralogy and Petrology 123, 40–60.

Barnes, C.G., Snoke, A.W., Harper, G.D., Frost, C.D., McFadden, R.R., Bushey, J.C., Barnes, M.A. W., 2006. Arc plutonism following regional thrusting; petrology and geochemistry of syn- and post-Nevadan plutons in the Siskiyou Mountains, Klamath Mountains province, California. In: Snoke, A.W., Barnes, C.G. (Eds.), Geological studies in the Klamath Mountains Province, California and Oregon: a volume in honor of William P. Irwin: Geological Society of America, 410, pp. 357–376.

Blome, C.D., Nestell, M.K., 1991. Evolution of a Permo-Triassic sedimentary melange, Grindstone Terrane, east-central Oregon. Geological Society of America Bulletin 103, 1280–1296.

Blome, C.D., Jones, D.L., Murchey, B.L., Liniecki, M., 1986. Geologic implications for radiolarian-bearing Paleozoic and Mesozoic rocks from the Blue Mountains province, Eastern Oregon. In: Vallier, T.L., Brooks, H.C. (Eds.), Geology of the Blue Mountains region of Oregon, Idaho, and Washington—geological implications of Paleozoic and Mesozoic paleontology and biostratigraphy, Blue Mountains province, Oregon and Idaho: U.S. Geological Survey Professional Paper, 1435, pp. 79–101.

Brooks, H.C., Vallier, T.L., 1978. Mesozoic rocks and tectonic evolution of eastern Oregon and western Idaho. In: Howell, D.G., McDougall, K.A. (Eds.), Mesozoic paleogeography

of the western United States: Los Angeles, The Pacific Section: Society of Economic Paleontologists and Mineralogists, pp. 133–145.
Brooks, H.C., Ferns, M.L., Avery, D.G., 1984. Geology and Gold Deposits Map of the Southwest Quarter of the Bates Quadrangle, Grant County. Oregon: Oregon Department of Geology and Mineral Industries Geological Map Series GMS–35, scale 1:24,000, 1 sheet.
Bryan, W.B., Finger, L.W., Chayes, F., 1969. Estimating proportions in petrographic mixing equations by least squares approximation. Science 163, 926–927.
Carpenter, P.S., Walker, N.W., 1992. Origin and tectonic significance of the Aldrich Mountains serpentinite matrix melange, northeastern Oregon. Tectonics 11, 690–708.
Chamberlain, K.R., Snoke, A.W., Barnes, C.G., Bushey, J.C., 2006. New U–Pb radiometric dates of the Bear Mountain intrusive complex, Klamath Mountains, California. In: Snoke, A.W., Barnes, C.G. (Eds.), Geological studies in the Klamath Mountains Province, California and Oregon: a volume in honor of William P. Irwin: Geological Society of America, 410, pp. 317–332.
Chiaradia, M., Fontboté, L., Beate, B., 2004. Cenozoic continental arc magmatism and associated mineralization in Ecuador. Mineralum Deposita 39, 204–222.
Chung, S.L., Liu, D.Y., Ji, J.Q., Chu, M.F., Lee, H.Y., Wen, D.J., Lo, C.H., Lee, T.Y., Qian, Q., Zhang, Q., 2003. Adakites from continental collision zones: melting of thickened lower crust beneath southern Tibet. Geology 31, 1021–1024.
Chung, S.L., Chu, M.F., Zhang, Y.Q., Xie, Y.W., Lo, C.H., Lee, T.Y., Lan, C.Y., Li, X.H., Zhang, Q., Wang, Y.Z., 2005. Tibetan tectonic evolution inferred from spatial and temporal variations in post-collisional magmatism. Earth-Science Reviews 68, 173–196.
Chung, S.L., Chu, M.F., Ji, J., O'Reilly, S.Y., Pearson, N.J., Liu, D.Y., Lee, T.Y., Lo, C.H., 2009. The nature and timing of crustal thickening in Southern Tibet: geochemical and zircon Hf isotopic constraints from postcollisional adakites. Tectonophysics 477, 36–48.
Cloos, M., 1993. Lithospheric buoyancy and collisional orogenesis: Subduction of oceanic plateaus, continental margins, island arcs, spreading ridges, and seamounts. Geological Society of America Bulletin 105, 715–737.
Connelly, J.N., 2001. Degree of preservation of igneous zonation in zircon as a signpost for concordancy in U/Pb geochronology. Chemical Geology 172, 25–39.
Coward, R.I., 1983. Structural geology, stratigraphy and petrology of the Elkhorn Ridge Argillite, in the Sumpter area, northeastern Oregon [PhD thesis]: Houston, TX, Rice University, pp. 144.
Dickinson, W.R., 1979. Mesozoic forearc basin in central Oregon. Geology 7, 166–170.
Dickinson, W.R., Thayer, T.P., 1978. Paleogeographic and paleotectonic implications of Mesozoic stratigraphy and structure in the John Day inlier of central Oregon. In: Howell, D.G., McDougall, K.A. (Eds.), Mesozoic paleogeography of the western United States, Society of Economic Paleontologists and Mineralogists: Pacific Section Paleogeography Symposium, 2, pp. 147–161.
Dickinson, W.R., Vigrass, L.W., 1965. Geology of the Suplee–Izee area, Crook, Grant, and Harney counties, Oregon. Oregon Department of Geology and Mineral Industries Bulletin 58, 109.
Dickinson, W.R., Helmold, K.P., Stein, J.A., 1979. Mesozoic lithic sandstones in central Oregon. Journal of Sedimentary Research 49, 501–516.
Dorsey, R.J., LaMaskin, T.A., 2007. Stratigraphic record of Triassic–Jurassic collisional tectonics in the Blue Mountains Province, northeastern Oregon. American Journal of Science 307, 1167–1193.
Drummond, M.S., Defant, M.J., 1990. A model for trondhjemite-tonalitedacite genesis and crustal growth via slab melting: Archean to modern comparisons. Journal of Geophysical Research 95, 21,503–21,521.
Evans, J.G., 1995. Pre-Tertiary deformation in the Desolation Butte Quadrangle, northeastern Oregon. In: Vallier, T.L., Brooks, H.C. (Eds.), Geology of the Blue Mountains Region of Oregon, Idaho and Washington; petrology and tectonic evolution of pre-Tertiary rocks of the Blue Mountains region: U. S. Geological Survey Professional Paper, 1438, pp. 305–330.
Ferns, M.L., Brooks, H.C., 1995. The Bourne and Greenhorn subterranes of the Baker Terrane, northeastern Oregon; implications for the evolution of the Blue Mountains island–arc system. In: Vallier, T.L., Brooks, H.C. (Eds.), Geology of the Blue Mountains Region of Oregon, Idaho and Washington; petrology and tectonic evolution of pre-Tertiary rocks of the Blue Mountains region: U.S. Geological Survey Professional Paper, 1438, pp. 331–358.
Ferns, M.L., Brooks, H.C., Avery, D.G., and Blome, C.D., 1987. Geology and mineral resources map of the Elkhorn Peak Quadrangle, Baker County, Oregon: Portland, OR, Oregon Department of Geology and Mineral Industries, GMS-41, scale 1:24,000, 1 sheet.
Fleck, R.J., Criss, R.E., 1985. Strontium and oxygen isotopic variations in Mesozoic and Tertiary plutons of central Idaho. Contributions to Mineralogy and Petrology 90, 291–308.
Gastil, R.G., 1975. Plutonic zones in the Peninsular Ranges of southern California and northern Baja California. Geology 3, 361–363.
Getty, S.R., Selverstone, J., Wernicke, B.P., Jacobsen, S.B., Aliberti, E., 1993. Sm–Nd dating of multiple garnet growth events in an arc–continent collision zone, northwestern U.S. Cordillera. Contributions to Mineralogy and Petrology 115, 45–47.
Gilluly, J., 1937. Geology and mineral resources of the Baker Quadrangle, Oregon. U. S. Geological Survey Bulletin 879, 199.
Gray, K.D., Oldow, J.S., 2005. Contrasting structural histories of the Salmon River belt and Wallowa terrane: implications for terrane accretion in northeastern Oregon and west-central Idaho. Geological Society of America Bulletin 117, 687–706.
Grimes, C.B., John, B.E., Kelemen, P.B., Mazdab, F., Wooden, J.L., Cheadle, M.J., Hanghoj, K., Schwartz, J.J., 2007. The trace element chemistry of zircons from oceanic crust: a method for distinguishing detrital zircon provenance. Geology 35, 643–646.
Grimes, C.B., John, B.E., Cheadle, M.J., Mazdab, F.K., Wooden, J.L., Swapp, S.M., Schwartz, J.J., 2009. On the occurrence, trace element geochemistry, and crystallization history of zircon from in situ ocean lithosphere. Contributions to Mineralogy and Petrology 158, 757–783.
Gromet, L.P., Silver, L.T., 1987. REE variations across the Peninsular Ranges batholith: implications for batholith petrogenesis and crustal growth in magmatic arcs. Journal of Petrology 28, 75–125.
Guo, Z.F., Wilson, M., Liu, J.Q., 2007a. Post-collisional adakites in south Tibet: products of partial melting of subduction-modified lower crust. Lithos 96, 205–224.
Guo, F., Nakamuru, E., Fan, W., Kobayoshi, K., Li, C., 2007b. Generation of Palaeocene adakitic andesites by magma mixing; Yanji area, NE China. Journal of Petrology 48, 661–692.
Harper, G.D., Wright, J.E., 1984. Middle to Late Jurassic tectonic evolution of the Klamath Mountains, California–Oregon. Tectonics 3, 759–772.
Harper, G.D., Saleeby, J.B., Heizler, M., 1994. Formation and emplacement of the Josephine Ophiolite and the Nevadan Orogeny in the Klamath Mountains, California–Oregon; U/Pb zircon and $^{40}Ar/^{39}Ar$ geochronology. Journal of Geophysical Research 99, 4293–4321.
Johnson, K., Barnes, C.G., 2002. Jurassic magmatism prior to and during terrane accretion in the Blue Mountains Province, NE Oregon. Geological Society of America Abstracts with Programs 34, 21–22.
Johnson, K., Schwartz, J.J., 2009. Overview of Jurassic–Cretaceous Magmatism in the Blue Mountains Province (NE Oregon & W Idaho): insights from New Pb/U (SHRIMP-RG) Age Determinations. Geological Society of America Abstracts with Programs 41, 182.
Johnson, K., Barnes, C.G., Miller, C.A., 1997. Petrology, geochemistry, and genesis of high-Al tonalite and trondhjemites of the Cornucopia stock, Blue Mountains, northeastern Oregon. Journal of Petrology 38, 1585–1611.
Johnson, S.E., Tate, M.C., Fanning, C.M., 1999. New geologic mapping and SHRIMP U–Pb zircon data in the Peninsular Ranges batholith, Baja California, Mexico: evidence for a suture? Geology 27, 743–746.
Johnson, K., Schwartz, J.J., Walton, C., 2007. Petrology of the Late Jurassic Sunrise Butte Pluton, eastern Oregon; a record of renewed Mesozoic arc activity? Geological Society of America Abstracts with Programs 39, 209.
Kay, S.M., Mpodozis, C., 2001. Central Andean ore deposits linked to evolving shallow subduction systems and thickening crust. GSA Today 11, 4–9.
Kays, M.A., Stimac, J.P., Goebel, P.M., 2006. Permian–Jurassic growth and amalgamation of the Wallowa composite terrane, northeastern Oregon. In: Snoke, A.W., Barnes, C.G. (Eds.), Geological studies in the Klamath Mountains Province, California and Oregon: a volume in honor of William P. Irwin: Geological Society of America, 410, pp. 465–494.
Kimbrough, D.L., Smith, D.P., Mahoney, J.B., Moore, T.E., Gastil, R.G., Ortega Rivera, M.A., Fanning, C.M., 2001. Forearc basin sedimentary response to rapid Late Cretaceous batholith emplacement in the Peninsular Ranges of southern and Baja California. Geology 29, 491–494.
Kurz, G.A., Northrup, C.J., Schmitz, M.D., 2009. High-precisions U–Pb dating of neoblastic sphene from mylonitic rocks of the Cougar Creek Complex, Blue Mountains Province, Oregon–Idaho: implications for the interplay between deformation and arc magmatism. Geological Society of America Abstracts with Programs 41, 182.
LaMaskin, T.A., Vervoort, J.D., Dorsey, R.J., Wright, J.E., 2011. Early Mesozoic paleogeography and tectonic evolution of the western United States: Insights from detrital zircon U-Pb geochronology, Blue Mountains Province, northeastern Oregon. Geological Society of America Bulletin 123 (9-10), 1939–1965.
LaMaskin, T.A., Dorsey, R., Vervoort, J., 2008. Early Mesozoic paleogeography and tectonic evolution of the Western United States; insights from detrital zircon U–Pb geochronology, Blue Mountains province, NE Oregon. Geological Society of America Abstracts with Programs 41, 9.
LaMaskin, T.A., Dorsey, R.J., Vervoort, J.D., 2009a. Initiation of the Cretaceous, Andean-type margin of the Western U.S. Cordillera: insights from detrital-zircon ages of the Coon Hollow Formation, Idaho, U.S.A. Geological Society of America Abstracts with Programs 41, 183.
LaMaskin, T.A., Schwartz, J.J., Dorsey, R.J., Snoke, A.W., Johnson, K., Vervoort, J.D., 2009b. Mesozoic sedimentation, magmatism, and tectonics in the Blue Mountains Province, northeastern Oregon. In: O'Connor, J.E., Dorsey, R.J., Madin, I.P. (Eds.), Volcanoes to vineyards: geologic field trips through the dynamic landscape of the Pacific Northwest: Geological Society of America Field Guide, 15, pp. 187–202.
Lee, R.G., 2004. The geochemistry, stable isotopic composition, and U–Pb geochronology of tonalite–trondhjemites within the accreted terrane, near Greer, north-central Idaho. [M.S. thesis] Washington State University, Pullman, WA, pp. 132.
Lund, K., 1995. Metamorphic and structural development of island–arc rocks in the Slate Creek–John Day Creek area, west-central Idaho. In: Vallier, T.L., Brooks, H.C. (Eds.), Geology of the Blue Mountains region of Oregon, Idaho, and Washington—petrology and tectonic evolution of pre-Tertiary rocks of the Blue Mountains region: U.S. Geological Survey Professional Paper, 1438, pp. 517–540.
Macpherson, C.G., Dreher, S.T., Thirlwall, M.F., 2006. Adakites without slab melting: high pressure differentiation of island arc magma, Mindanao, the Philippines. Earth and Planetary Science Letters 243, 581–593.
Manduca, C.A. 1988, Geology and geochemistry of the oceanic arc–continent boundary in the western Idaho batholith near McCall. [Ph.D. thesis] California Institute of Technology, pp. 272.
Manduca, C.A., Kuntz, M.A., Silver, L.T., 1993. Emplacement and deformation history of the western margin of the Idaho batholith near McCall, Idaho: influence of a major terrane boundary. Geological Society of America Bulletin 105, 749–765.
Mantle, G.W., Collins, W.J., 2008. Quantifying crustal thickness variations in evolving orogens: correlation between arc basalt composition and Moho depth. Geology 36, 87–90.
Martin, H., 1987. Petrogenesis of Archaean trondhjemites, tonalites, and granodiorites from eastern Finland: major and trace element geochemistry. Journal of Petrology 28, 921–953.

Martin, H., 1999. Adakitic magmas: modern analogues of Archean granitoids. Lithos 46, 411–429.
McLelland, J.M., Bickford, M.E., Hill, B.M., Clechenko, C.C., Valley, J.W., Hamilton, M.A., 2004. Direct dating of Adirondack massif anorthosite by U–Pb SHRIMP analysis of igneous zircon: implications for AMCG complexes. Geological Society of America Bulletin 116, 1299–1317.
McClelland, W.C., Oldow, J.S., 2007. Late Cretaceous truncation of the western Idaho shear zone in the central North American Cordillera. Geology 35, 723–726.
Miyashiro, A., 1974. Volcanic rock series in island arcs and active continental margins. American Journal of Science 274, 321–355.
Moyen, J.F., 2009. High Sr/Y and La/Yb ratios: the meaning of the "adakitic signature". Lithos 112, 556–574.
Muir, R.J., Ireland, T.R., Weaver, S.D., Bradshaw, J.D., Waight, T.E., Jongens, R., Eby, G.N., 1997. SHRIMP U–Pb geochronology of Cretaceous magmatism in northwest Nelson–Westland, South Island, New Zealand. New Zealand Journal of Geology and Geophysics 40, 453–463.
Muir, R.J., Ireland, T.R., Weaver, S.D., Bradshaw, J.D., Evans, J.A., Eby, G.N., Shelley, D., 1998. Geochronology and geochemistry of a Mesozoic magmatic arc system, Fiordland, New Zealand. Journal of the Geological Society of London 155, 1037–1053.
Mullen, E.D., 1978. Geology of the Greenhorn Mountains, northeastern Oregon. [M.S. thesis] Corvallis, Oregon State University, pp. 372.
Nestell, M.K., 1983. Permian foraminiferal faunas of central and eastern Oregon. Geological Society of America Abstracts with Programs 15, 371.
Nestell, M.K., Nestell, G.P., 1998. Middle Permian conodonts and Tethyan fusulinaceans associated with possible seamount debris in Oregon. Geological Society of America Abstracts with Programs 30, 151–152.
Nestell, M.K., Orchard, M.J., 2000. Late Paleozoic and middle Late Triassic conodont assemblages from the Baker Terrane, eastern Oregon. Geological Society of America Abstracts with Programs 32, 59.
Nestell, M.K., Lambert, L.L., Wardlaw, B.R., 1995. Pennsylvanian conodonts and fusulinaceans of the Baker Terrane, eastern Oregon. Geological Society of America Abstracts with Programs 27, 76.
Pardee, J.T., Hewett, D.F., 1914. Geology and mineral resources of the Sumpter Quadrangle, Oregon. Oregon Bureau of Mines and Geology 1, 3–128.
Petford, N., Atherton, M., 1996. Na-rich partial melts from newly underplated basaltic crust; the Cordillera Blanca Batholith, Peru. Journal of Petrology 37, 1491–1521.
Rapp, R.P., Watson, E.B., Miller, C.F., 1991. Partial melting of amphibolite/eclogite and the origin of Archean trondhjemites and tonalites. Precambrian Research 51, 1–25.
Rooney, T.O., Franceschi, P., Hall, C.M., 2011. Water-saturated magmas in the Panama Canal region: a precursor to adakite-like magma generation? Contributions to Mineralogy and Petrology 161, 373–388.
Rudnick, R., 1995. Making continental crust. Nature 378, 571–578.
Rushmer, T., 1991. Partial melting of two amphibolites: contrasting experimental results under fluid-absent conditions. Contributions to Mineralogy and Petrology 107, 41–59.
Saleeby, J.B., Harper, G.D., Snoke, A.W., Sharp, W.D., 1982. Time relations and structural-stratigraphic patterns in ophiolite accretion, west central Klamath Mountains, California. Journal of Geophysical Research 87, 3831–3848.
Schwartz, J.J., Johnson, K., 2009. Origin of paired Late Jurassic high and low Sr/Y magmatic belts in the Blue Mountains Province, NE Oregon. Geological Society of America Abstracts with Programs 41, 182.
Schwartz, J.J., Snoke, A.W., Frost, C.D., Barnes, C.G., Gromet, L.P., Johnson, K., 2010. Analysis of the Wallowa–Baker terrane boundary: implications for tectonic accretion in the Blue Mountains province, northeastern Oregon. Geological Society of America Bulletin 122, 517–536.
Schwartz, J.J., Snoke, A.W., Cordey, F., Johnson, K., Frost, C.D., Barnes, C.G., LaMaskin, T.A., Wooden, J.L., 2011. Late Jurassic magmatism, metamorphism and deformation in the Blue Mountains province, northeast Oregon. Geological Society of America Bulletin 123 (9-10), 2083–2111.
Selverstone, J., Wernicke, B., Aliberti, E.A., 1992. Intracontinental subduction and hinged unroofing along the Salmon River suture zone, west central idaho. Tectonics 11, 124–144.
Silberling, N.J., Jones, D.L., Blake, M.C., and Howell, D.G., 1987. Lithotectonic terrane map of the western conterminous United States. U. S. Geological Survey Miscellaneous Field Studies Map MF-1874-C, scale 1:250,000, with 20 p. pamphlet.
Silver, L.T., Chappell, B.W., 1988. The Peninsular Ranges batholith: an insight into the evolution of the Cordilleran batholiths of southwestern North America. Transactions of the Royal Society of Edinburgh 79, 105–121.
Silver, L.T., Taylor Jr., H.P., Chappell, B.W., 1979. Some petrological, geochemical, and geochronological observations of the Peninsular Ranges batholith near the international border of the U.S.A. and Mexico. In: Abbott, P.L, Todd, V.R. (Eds.), Mesozoic crystalline rocks: Peninsular Ranges batholith and pegmatites and Point Sal Ophiolite: San Diego State University, Department of Geological Sciences, pp. 83–110.
Smithies, R.H., 2000. The Archaean tonalite–trondhjemite–granodiorite (TTG) series is not an analogue of Cenozoic adakite. Earth and Planetary Science Letters 182, 115–125.
Snee, L.W., Lund, K., Sutter, J.F., Balcer, D.E., Evans, K.V., 1995. An $^{40}Ar/^{39}Ar$ chronicle of the tectonic development of the Salmon River suture zone, western Idaho. U. S. Geological Survey Professional Paper 1438, 359–414.
Snee, L.W., Davidson, G.F., Unruh, D.M., 2007. Geological, geochemical, and $^{40}Ar/^{39}Ar$ and U-Pb thermochronological constraints for the tectonic development of the Salmon River suture zone near Orofino, Idaho. In: Kuntz, M.A., Snee, L.W. (Eds.), Geological studies of the Salmon River suture zone and adjoining areas, west-central Idaho and eastern Oregon: U.S. Geological Survey Professional Paper, 1738, pp. 51–94.
Snoke, A.W., 1977. A thrust plate of ophiolitic rocks in the Preston Peak area, Klamath Mountains, California. Geological Society of America Bulletin 88, 1641–1659.
Snoke, A.W., Quick, J.E., Bowman, H.R., 1981. Bear Mountain igneous complex, Klamath Mountains, California: an ultrabasic to silicic calcalkaline suite. Journal of Petrology 22, 501–552.
Sun, S.S., McDonough, W.F., 1989. Chemical and isotopic systematics of oceanic basalts; implications for mantle composition and processes. Geological Society Special Publications 42, 313–345.
Taubeneck, W.H., 1995. A closer look at the Bald Mountain Batholith, Elkhorn Mountains, and some comparisons with the Wallowa Batholith, Wallowa Mountains, northeastern Oregon. In: Vallier, T.L., Brooks, H.C. (Eds.), Geology of the Blue Mountains region of Oregon, Idaho, and Washington; petrology and tectonic evolution of pre-Tertiary rocks of the Blue Mountains region: U.S. Geological Survey Professional Paper, 1438, pp. 45–138.
Taylor, H.P., Silver, L.T., 1978. Oxygen isotope relationships in plutonic igneous rocks of the Peninsular Ranges batholith, southern and Baja California. In: Zartman, R.E. (Ed.), Short papers of the fourth international conference, geochronology, cosmochronology, isotope geology: U.S. Geological Survey Open-File Report 78-0701, pp. 423–426.
Tomaschek, F., Kennedy, A.K., Villa, I.M., Lagos, M., Ballhaus, C., 2003. Zircons from Syros, Cyclades, Greece; recrystallization and mobilization of zircon during high-pressure metamorphism. Journal of Petrology 44, 1977–2002.
Tulloch, A.J., 1983. Granitoid rocks of New Zealand—a brief review. Geological Society of America Memoir 159, 5–20.
Tulloch, A.J., 1988. Batholiths, plutons and suites: nomenclature for granitoid rocks of Westland-Nelson, New Zealand. New Zealand Journal of Geology and Geophysics 31, 505–509.
Tulloch, A.J., Kimbrough, D.L., 2003. Paired plutonic belts in convergent margins and the development of high Sr/Y magmatism: Peninsular Ranges batholith of Baja-California and Median batholith of New Zealand. In: Johnson, S.E., Paterson, S.R., Fletcher, J.M., Girty, G.H., Kimbrough, D.L., Martín-Barajas, A. (Eds.), Tectonic evolution of northwestern México and the southwestern USA: Boulder, Colorado: Geological Society of America Special Paper, 374, pp. 275–295.
Tulloch, A.J., Rabone, S.D.C., 1993. Mo-bearing granodiorite porphyry plutons of the Early Cretaceous Separation Point suite west Nelson, New Zealand. New Zealand Journal of Geology and Geophysics 36, 401–408.
Tumpane, K.P., Schmitz, M.D., 2009. New geochronological constraints on the timing of deposition in the Coon Hollow and Weatherby Formations, and correlations between the Wallowa and Olds Ferry Terranes, Blue Mountains Province, Northern U.S. Cordillera. Geological Society of America Abstracts with Programs 41, 182.
Unruh, D.M., Lund, K., Kuntz, M.A., Snee, L.W., 2008. Uranium–lead zircon ages and Sr, Nd, and Pb isotope geochemistry of selected plutonic rocks from western Idaho. U. S. Geological Survey Open-File Report, 1142, pp. 1–37.
Vallier, T.L., 1977. The Permian and Triassic Seven Devils Group, western Idaho and northeastern Oregon. U. S. Geological Survey Bulletin B1437, 1–58.
Vallier, T.L., 1995. Petrology of pre-Tertiary igneous rocks in the Blue Mountains region of Oregon, Idaho, and Washington; implications for the geologic evolution of a complex island arc. In: Vallier, T.L., Brooks, H.C. (Eds.), Geology of the Blue Mountains Region of Oregon, Idaho and Washington; petrology and tectonic evolution of pre-Tertiary rocks of the Blue Mountains region: U. S. Geological Survey Professional Paper, 1438, pp. 125–209.
Vallier, T.L., Batiza, R., 1978. Petrogenesis of spilite and keratophyre from a Permian and Triassic volcanic arc terrane, eastern Oregon and western Idaho, U.S.A. Canadian Journal of Earth Sciences — Journal Canadien des Sciences de la Terre 15, 1356–1369.
Vallier, T.L., Brooks, H.C., Thayer, T.P., 1977. Paleozoic rocks of eastern Oregon and western Idaho. Society of Economic Paleontologists and Mineralogists 455–466.
Walawender, M.J., Gastil, R.G., Clinkenbeard, J.P., McCormick, W.V., Eastman, B.G., Wernicke, R.S., Wardlaw, M.S., Gunn, S.H., Smith, B.M., 1990. Origin and evolution of the zoned La Posta-type plutons, eastern Peninsular Ranges batholith, southern and Baja California. In: Anderson, J.L. (Ed.), The nature and origin of Cordilleran magmatism: Geological Society of America Memoir, 174, pp. 1–18.
Walker, N.W., 1986. U/Pb geochronologic and petrologic studies in the Blue Mountains Terrane, northeastern Oregon and westernmost-central Idaho; implications for pre-Tertiary tectonic evolution, [Ph.D. thesis], Santa Barbara, University of California, pp. 1–224.
Walker, N.W., 1989. Early Cretaceous initiation of post-tectonic plutonism and the age of the Connor Creek Fault, northeastern Oregon. Geological Society of America Abstracts with Programs 21, 155.
Walker, N.W., 1995. Tectonic implications of U–Pb zircon ages of the Canyon Mountain Complex, Sparta Complex, and related metaplutonic rocks of the Baker Terrane, northeastern Oregon. In: Vallier, T.L., Brooks, H.C. (Eds.), Geology of the Blue Mountains region of Oregon, Idaho and Washington; petrology and tectonic evolution of pre-Tertiary rocks of the Blue Mountains region: U.S. Geological Survey Professional Paper, 1438, pp. 247–269.
Wang, Q., McDermott, F., Xu, J.F., Bellon, H., Zhu, Y.T., 2005. Cenozoic K-rich adakitic volcanic rocks in the Hohxil area, northern Tibet: lower crustal melting in an intracontinental setting. Geology 33, 464–468.
Wang, Q., Wyman, A., Xu, J.F., Jian, P., Zhao, Z.H., Li, C.F., Xu, W., Ma, J.L., He, B., 2007. Early Cretaceous adakitic granites in the Northern Dabie complex, central China: implications for partial melting and delamination of thickened lower crust. Geochimica et Cosmochimica Acta 71, 2609–2636.
Wang, Q., Wyman, D.A., Xu, J.F., Dong, Y.H., Vasconcelos, P.M., Pearson, N., Wan, Y.S., Dong, H., Li, C.F., Yu, Y.S., Zhu, T.X., Feng, X.T., Zhang, Q.Y., Zi, F., Chu, Z.Y., 2008. Eocene melting of subducting continental crust and early uplifting of central Tibet: evidence from central-western Qiangtang high-K calc-alkaline andesites, dacites and rhyolites. Earth and Planetary Science Letters 272, 158–171.

Wheeler, G.R., 1976, Geology of the Vinegar Hill area, Grant County, Oregon: [Ph.D. dissertation], Seattle, University of Washington, pp. 1–94.
Winther, K.T., Newton, R.C., 1991. Experimental melting of hydrous low-K tholeiite: evidence on the origin of Archaean cratons. Bulletin of the Geological Society of Denmark 39, 213–228.
Wolf, M.B., Wyllie, P.J., 1993. Garnet growth during amphibolite anatexis: implications of a garnetiferous restite. Journal of Geology 101, 357–373.
Wolf, M.B., Wyllie, P.J., 1994. Dehydration-melting of amphibolite at 10 kbar: the effects of temperature and time. Contributions to Mineralogy and Petrology 115, 369–383.
Xu, W.C., Zhang, H.F., Guo, L., Yuan, H.L., 2009. Miocene high Sr/Y magmatism, south Tibet: product of partial melting of subducted Indian continental crust and its tectonic implication. Lithos 114, 293–306.
Yogodzinski, G.M., Kelemen, P.B., 1998. Slab melting in the Aleutians: implications of an ion probe study of clinopyroxene in primitive adakite and basalt. Earth and Planetary Science Letters 158, 53–65.

Further reading

Alexander, R., Schwartz, J.J., 2009. Detrital zircon geochronology of Permian–Triassic metasedimentary rocks in the Baker terrane, Blue Mountains Province, NE Oregon. Geological Society of America Abstracts with Programs 41, 294.
Bouvier, A., Vervoort, J.D., Patchett, P.J., 2008. The Lu–Hf and Sm–Nd isotopic composition of CHUR: constraints from unequilibrated chondrites and implications for the bulk composition of terrestrial planets. Earth and Planetary Science Letters 273, 48–57.
Chu, N.C., Taylor, R.N., Chavagnac, V., Nesbitt, R.W., Boella, R.M., Milton, J.A., German, C. R., Bayon, G., Burton, K., 2002. Hf isotope ratio analysis using multi-collector inductively coupled plasma mass spectrometry: an evaluation of isobaric interference corrections. Journal of Analytical Atomic Spectrometry 17, 1567–1574.
Claiborne, L.L., Miller, C.F., Walker, B.A., Wooden, J.L., Mazdab, F., Bea, F., 2006. Tracking magmatic processes through Zr/Hf ratios in rocks and Hf and Ti zoning in zircons: an example from the Spirit Mountain batholith, Nevada. Mineralogical Magazine 70, 517–543.
Compston, W., Williams, I.S., Meyer, C.E., 1984. U–Pb geochronology of zircons from lunar breccia 73217 using a sensitive high mass-resolution ion microprobe. Journal of Geophysical Research B 89, 525–534.
DePaolo, D.J., 1981. Trace element and isotopic effects of combined wallrock assimilation and fractional crystallization. Earth and Planetary Science Letters 53, 189–202.
Drake, M.J., Weill, D.F., 1975. Partition of Sr, Ba, Ca, Y, Eu^{2+}, Eu^{3+}, and Other REE between plagioclase feldspar and magmatic liquid — experimental study. Geochimica et Cosmochimica Acta 39, 689–712.
Evans, J.G., 1989. Geologic map of the Desolation Butte Quadrangle, Grant and Umatilla counties, Oregon: Reston, VA, U. S. Geological Survey Geologic Quadrangle GQ-1654, scale 1:62,500, 1 sheet.
Ewart, A., Griffin, W.L., 1994. Application of proton-microprobe data to trace-element partitioning in volcanic-rocks. Chemical Geology 117, 251–284.
Frost, B.R., Barnes, C.G., Collins, W.J., Arculus, R.J., Ellis, D.J., Frost, C.D., 2001. A geochemical classification for granitic rocks. Journal of Petrology 42, 2033–2048.
Fujimaki, H., Tatsumoto, M., Aoki, K.-i., 1984. Partition coefficients of Hf, Zr, and REE between phenocrysts and groundmasses. Journal of Geophysical Research 89, 662–672.
Gehrels, G.E., Valencia, V., Ruiz, J., 2008. Enhanced precision, accuracy, efficiency, and spatial resolution of U–Pb ages by laser ablation-multicollector-inductively coupled plasma-mass spectrometry. Geochemistry, Geophysics, Geosystems 9, Q03017. doi:10.1029/2007GC001805.
Gerdes, A., Zeh, A., 2009. Zircon formation versus zircon alteration — new insights from combined U–Pb and Lu–Hf in-situ LA-ICP-MS analyses, and consequences for the interpretation of Archean zircon from the Central Zone of the Limpopo Belt. Chemical Geology 261, 230–243.
Griffin, W.L., Wang, X., Jackson, S.E., Pearson, N.J., O'Reilly, S.Y., Xu, X., Zhou, X., 2002. Zircon chemistry and magma mixing, SE China: in situ analysis of Hf isotopes, Tonglu and Pingtan igneous complexes. Lithos 61, 237–269.
Hawkesworth, C.J., Kemp, A.I.S., 2006. Using hafnium and oxygen isotopes in zircons to unravel the record of crustal evolution. Chemical Geology 226, 144–162.
Housen, B.A., 2007. Paleomagnetism of Mesozoic–Cenozoic rocks of the Blue Mountains, Oregon. Geological Society of America Abstracts with Programs 39, 207–208.
Housen, B.A., Dorsey, R.J., 2005. Paleomagnetism and tectonic significance of Albian and Cenomanian turbidites, Ochoco Basin, Mitchell Inlier, central Oregon. Journal of Geophysical Research 110, B07102. doi:10.1029/2004JB003458.
Iizuka, T., Hirata, T., 2005. Improvements of precision and accuracy in in situ Hf isotope microanalysis of zircon using the laser ablation MC-ICPMS technique. Chemical Geology 220, 121–137.
Jenner, G.A., Foley, S.F., Jackson, S.E., Green, T.H., Fryer, B.J., Longerich, H.P., 1994. Determination of partition coefficients for trace elements in high pressure–temperature experimental run products by laser ablation microprobe-inductively coupled plasma-mass spectrometry (LAM-ICP-MS). Geochimica et Cosmochimica Acta 57, 5099–5103.
Kemp, A.I.S., Foster, G.L., Schersten, A., Whitehouse, M.J., Darling, J., Storey, C., 2009. Concurrent Pb–Hf isotope analysis of zircon by laser ablation multi-collector ICP-MS, with implications for the crustal evolution of Greenland and the Himalayas. Chemical Geology 261, 244–263.
Kimbrough, D.L., Moore, T.E., 2003. Ophiolite and volcanic arc assemblages on the Vizcaino Peninsula and Cedros Island, Baja California Sur, Mexico: Mesozoic forearc lithosphere of the Cordilleran magmatic arc. In: Johnson, S.E., Paterson, S.R., Fletcher, J., Girty, G.H., Kimbrough, D.L., Martin-Barajas, A. (Eds.), Tectonic evolution of northwestern Mexico and the southwestern USA: a volume in honor of R. Gordon Gastil: Geological Society of America Special Paper, 374, pp. 43–71.
Klein, M., Stosch, H.G., Seck, H.A., 1997. Partitioning of high field-strength and rare-earth elements between amphibole and quartz-dioritic to tonalitic melts: an experimental study. Chemical Geology 138, 257–271.
Langmuir, C.H., 1989. Geochemical consequences of in situ crystallization. Nature 340, 199–205.
Ludwig, K.R., 2001. SQUID 1.02. Berkeley Geochronology Center Special Publication, 2, pp. 1–19.
Ludwig, K.R., 2003. Isoplot 3.00: a geochronological toolkit for Microsoft Excel. Berkeley Geochronology Center Special Publication, 4, pp. 1–70.
Luhr, J.F., Carmichael, I.S.E., 1980. The Colima volcanic complex, Mexico. I: post-caldera andesites from Volcan Colima. Contributions to Mineralogy and Petrology 71, 343–372.
Mazdab, F.K., 2009. Characterization of flux-grown trace element-doped titanite using the high-mass-resolution ion microprobe (SHRIMP-RG). Canadian Mineralogist 47, 813–831.
Mazdab, F., Wooden, J.L., 2006. Trace element analysis in zircon by ion microprobe (SHRIMP-RG); technique and applications. Geochimica et Cosmochimica Acta 70, A405 (2006 Goldschmidt abstract volume).
Patchett, P.J., 1983. Importance of the Lu–Hf isotopic system in studies of planetary chronology and chemical evolution. Geochimica and Cosmochimica Acta 47, 81–91.
Patchett, P.J., Tatsumoto, M., 1980. A routine high-precision method for Lu–Hf isotope geochemistry and chronology. Contributions to Mineralogy and Petrology 75, 263–267.
Pearce, J.A., Norry, M.J., 1979. Petrogenetic implications of Ti, Zr, Y, and Nb variations in volcanic rocks. Contributions to Mineralogy and Petrology 69, 33–47.
Philpotts, J.A., Schnetzler, C.C., 1970. Phenocryst-matrix partition coefficients for K, Rb, Sr and Ba, with applications to anorthosite and basalt genesis. Geochimica et Cosmochimica Acta 34, 307–322.
Rollinson, H.R., 1993. Using Geochemical Data: Evaluation, Presentation, Interpretation. Longman Scientific and Technical, Essex, England.
Scherer, E., Munker, C., Mezger, K., 2001. Calibration of the lutetium–hafnium clock. Science 293, 683–687.
Schnetzler, C.C., Philpotts, J.A., 1970. Partition coefficients of rare-earth elements between igneous matrix material and rock-forming mineral phenocrysts; II. Geochimica et Cosmochimica Acta 34, 331–340.
Segal, I., Halicz, L., Platzner, I.T., 2003. Accurate isotope ratio measurements of ytterbium by multiple collection inductively coupled plasma mass spectrometry applying erbium and hafnium in an improved double external normalization procedure. Journal of Analytical Atomic Spectrometry 18, 1217–1223.
Sisson, T.W., 1994. Hornblende-melt trace-element partitioning measured by ion microprobe. Chemical Geology 117, 331–344.
Slama, J., Kosler, J., Condon, D.J., Crowley, J.L., Gerdes, A., Hanchar, J.M., Horstwood, M.S. A., Morris, G.A., Nasdala, L., Norberg, N., Schaltegger, U., Schoene, B., Tubrett, M.N., Whitehouse, M.J., 2008. Plesovice zircon — a new natural reference material for U–Pb and Hf isotopic microanalysis. Chemical Geology 249, 1–35.
Snoke, A.W., Barnes, C.G., 2006. The development of tectonic concepts for the Klamath Mountains province, California and Oregon. In: Snoke, A.W., Barnes, C.G. (Eds.), Geological studies in the Klamath Mountains Province, California and Oregon: a volume in honor of William P. Irwin: Geological Society of America, 410, pp. 1–29.
Stacey, J.S., Kramers, J.D., 1975. Approximation of terrestrial lead isotope evolution by a two stage model. Earth and Planetary Science Letters 26, 207–221.
Taubeneck, W.H., 1964. Cornucopia stock, Wallowa Mountains, northeastern Oregon; field relations. Geological Survey of America Bulletin 75, 1093–1115.
Taubeneck, W.H., 1967. Petrology of the Cornucopia tonalite unit, Cornucopia stock, Wallowa Mountains, northeastern Oregon. Geological Society of America Special Paper 91, 1–56.
Tera, F., Wasserburg, G.J., 1972. U–Th–Pb systematics in three Apollo 14 basalts and the problem of initial Pb in lunar rocks. Earth and Planetary Science Letters 14, 281–304.
Vervoort, J.D., Patchett, P.J., Söderlund, U., Baker, M., 2004. The isotopic composition of Yb and the precise and accurate determination of Lu concentrations and Lu/Hf ratios by isotope dilution using MC-ICPMS. Geochemistry, Geophysics, Geosystems doi 2004GC000721RR.
Watson, E.B., Green, T.H., 1981. Apatite/liquid partition coefficients for the rare earth elements and strontium. Earth and Planetary Science Letters 56, 405–421.
Williams, I.S., 1998. U–Th–Pb geochronology by ion microprobe. In: McKibben (Ed.), Applications of microanalytical techniques to understanding mineralization processes: Reviews in Economic Geology, 7, pp. 1–35.
Wooden, J.L., Mazdab, F.K., Barth, A.P., Miller, C.F., Lowery, L.E., 2006. Temperatures (Ti) and compositional characteristics of zircon: early observations using high mass resolution on the USGS-Stanford SHRIMP-RG. Geochimica et Cosmichimica Acta 70, A707 (2006 Goldschmidt abstract volume).
Woodhead, J.D., Hergt, J.M., 2005. A preliminary appraisal of seven natural zircon reference materials for in situ Hf isotope determination. Geostandards and Geoanalytical Research 29, 183–195.
Woodhead, J.D., Hergt, J., Shelley, M., Eggins, S., Kemp, R., 2004. Zircon Hf-isotope analysis with an excimer laser, depth profiling, ablation of complex geometries, and concomitant age estimation. Chemical Geology 209, 121–135.
Wu, F.Y., Yang, Y.H., Xie, L.W., Yang, J.H., Xu, P., 2006. Hf isotopic compositions of the standard zircons and baddeleyites used in U–Pb geochronology. Chemical Geology 234, 105–126.
Muir, R.J., Weaver, S.D., Bradshaw, J.D., Eby, G.N., Evans, J.A., 1995. The Cretaceous Separation Point batholith, New Zealand: granitoid magmas formed by melting of a mafic lithosphere. Journal of the Geological Society of London 152, 689–701.